Research Square

Preprints are preliminary reports that have not undergone peer review.
They should not be considered conclusive, used to inform clinical practice,
or referenced by the media as validated information.

Choline Metabolism as a Targetable Driver of Inflammatory Osteoarthritis

Monica Guma

mguma@health.ucsd.edu

University California San Diego

Rocio Paz-Gonzalez

University of California San Diego

Martha Cedeño

University of California San Diego

Alecio F Lombardi

University of California San Diego

Harsha Gouda

Skaggs School of Pharmacy and Pharmaceutical Sciences, University of California San Diego
https://orcid.org/0000-0003-4511-5875

Helena Mannochio-Russo

UC San Diego https://orcid.org/0000-0002-4961-2353

Vincent Charron-Lamoureux

University of California San Diego https://orcid.org/0000-0001-9440-7036

Roxana Coras

University of California San Diego

Rebecca Latham

University of California San Diego

Jessica Murillo-Saich

University of California San Diego

Marta Sala-Climent

University of California San Diego

Nathan Argel

University of California San Diego

Zhuoran Chen

University of California San Diego

Julius Agongo

University of California San Diego

Shanzay Ahmed

University of California San Diego

Lucia Lourido
Instituto de Investigación Biomédica de A Coruña (INIBIC), Hospital Universitario A Coruña (HUAC), Universidad de Coruña (UDC)
Valentina Calamia
Instituto de Investigación Biomédica de A Coruña
Adnan Cutuk
VA San Diego Healthcare System
Robert Sah
https://orcid.org/0000-0002-5493-9502
Ignacio Rego Perez
Instituto de Investigación Biomédica de A Coruña (INIBIC), Hospital Universitario A Coruña (HUAC), Universidad de Coruña (UDC) https://orcid.org/0000-0003-1754-1164
Cristina Ruiz-Romero
Instituto de Investigación Biomédica de A Coruña https://orcid.org/0000-0001-7649-9803
Francisco J. Blanco
Eric Y Chang
University of California San Diego
Elsa Sanchez-Lopez
University of California San Diego https://orcid.org/0000-0002-4236-1985
Ru Liu-Bryan
Nancy Lane
University of Davis School of Medicine https://orcid.org/0000-0002-0177-2198
Pieter Dorrestein
The Univeristy of Califronia, San Diego https://orcid.org/0000-0002-3003-1030

Article

Keywords:

Posted Date: November 20th, 2026

DOI: https://doi.org/10.21203/rs.3.rs-11435219/v1

License: This work is licensed under a Creative Commons Attribution 4.0 International License.
Read Full License

Additional Declarations: There is **NO** Competing Interest.

Title: Choline Metabolism as a Targetable Driver of Inflammatory Osteoarthritis

Authors: Rocio Paz-Gonzalez[1,2], Martha Cedeño[1], Alecio F Lombardi[3], Harsha Gouda[4], Helena Mannochio-Russo[4], Vincent Charron-Lamoureux[4], Roxana Coras[1], Rebecca Latham[1], Jessica Murillo-Saich[1], Marta Sala-Climent[1] , Nathan Argel[1], Zhuoran Chen[5], Julius Agongo[4], Shanzay Ahmed[1], Lucia Lourido[2,6], Valentina Calamia[2], Adnan Cutuk[7], Robert Sah[8], Ignacio Rego[2], Cristina Ruiz-Romero[2,6], Francisco J Blanco[2], Eric Y Chang[3], Elsa Sanchez-Lopez[5], Ru Bryan[1], Nancy E Lane[9], Pieter C. Dorrestein[4], Monica Guma[1,#]

Affiliations:
[1]Department of Medicine, School of Medicine, University of California San Diego, San Diego, CA 92093, USA.
[2]Grupo de Investigación de Reumatología (GIR), Instituto de Investigación Biomédica de A Coruña (INIBIC), Hospital Universitario A Coruña (HUAC), Universidad de Coruña (UDC), A Coruña, Spain.
[3]Department of Radiology, University of California San Diego, San Diego, California, USA.
[4]Skaggs School of Pharmacy and Pharmaceutical Sciences, University of California San Diego, San Diego, CA 92093, USA.
[5]Department of Orthopedics, University of California San Diego, San Diego, California, USA.
[6]Centro de Investigación Biomédica en Red de Bioingeniería, Biomateriales y Nanomedicina (CIBER-BBN), Madrid, España.
[7]Department of Orthopedics, VA San Diego Healthcare System, CA, San Diego, California, USA.
[8]Department of Bioengineering, University of California San Diego, CA, USA.
[9]Department of Medicine, University of California, Davis, California, USA.

[#]**Corresponding author:** mguma@health.ucsd.edu

Running title: Choline–ChoKα Axis in Osteoarthritis Synovitis

Key words: osteoarthritis, synovitis, choline, metabolomics, dietary choline, choline kinase alpha, inflammation, disease progression

ABSTRACT

Osteoarthritis (OA) is a leading cause of pain and disability worldwide, yet disease-modifying treatments remain unavailable. Synovitis contributes to OA pain and progression, but its metabolic drivers remain poorly understood. Using untargeted plasma metabolomics in 471 participants in the Osteoarthritis Initiative (OAI) cohort, we identified circulating choline as the only metabolite shared by two distinct MRI-defined synovitis phenotypes and found that it was associated with radiographic progression over 48 months. A plasma metabolomic signature of choline-rich foods linked potential dietary sources of choline to circulating levels and synovitis. In human synovial tissue, we identified choline transport and phosphorylation machinery in fibroblasts and demonstrated that increased choline availability promotes their inflammatory and migratory responses. Conversely, pharmacological inhibition of choline kinase α attenuated pathogenic fibroblast behavior and cartilage inflammatory responses and reduced synovitis and structural joint damage in two mouse models. These findings identify choline metabolism as a previously unrecognized, therapeutically targetable pathway in OA, connecting systemic metabolism and potential dietary influences to synovial inflammation and joint pathology.

INTRODUCTION

Osteoarthritis (OA) is the most prevalent joint disease worldwide and a leading cause of chronic pain and disability[1, 2]. Although traditionally characterized by cartilage degeneration, OA is now recognized as a whole-joint disease in which the synovium plays an active role in shaping symptoms and disease progression[3-5], highlighting inflammation as a clinically relevant component of disease pathogenesis[6-8]. Synovial inflammation (synovitis) can be assessed on non-contrast magnetic resonance imaging (MRI) using two complementary features: effusion-synovitis, reflecting joint fluid accumulation and Hoffa-synovitis, reflecting signal changes in the infrapatellar fat pad, both scored with the MRI Osteoarthritis Knee Score (MOAKS).

Beyond its association with pain and cartilage loss, MRI-defined synovitis has been linked to the development of incident radiographic OA and subsequent structural progression[9-11]. Understanding the mechanisms underlying synovial inflammation may therefore open new therapeutic opportunities to modify the course of OA by targeting synovitis.

Growing evidence suggests that synovial inflammation in OA is influenced not only by local joint damage but also by systemic metabolic and environmental factors. At the tissue level, inflamed OA synovium exhibits distinct metabolic profiles compared with non-inflamed synovium[12], while systemic factors such as obesity, metabolic syndrome and dietary patterns have been associated with OA incidence and progression[6, 13, 14]. Together, these findings raise the possibility that circulating metabolites may link systemic metabolic influences on local synovial inflammation. However, which circulating metabolites are associated with synovitis and whether their metabolic pathways contribute to inflammatory responses within the joint remain poorly understood[15].

We hypothesized that circulating metabolites are associated with synovial inflammation and may contribute to local inflammatory processes and OA progression. To test this hypothesis, we integrated untargeted plasma metabolomics with demographic, clinical and MRI-defined synovitis data from participants with radiographic knee OA (rKOA) in the Osteoarthritis Initiative (OAI) cohort, followed by investigation of the identified metabolic pathway in human synovial tissue, primary human synovial fibroblasts and experimental OA models. We identified circulating choline as a metabolite associated with synovitis and subsequent structural progression, revealing a functionally relevant choline–ChoKα axis with potential therapeutic implications for OA.

RESULTS

Plasma metabolomics profiling identifies free choline as a circulating biomarker of synovitis in radiographic knee osteoarthritis

To identify circulating metabolites associated with synovial inflammation, we analyzed baseline plasma samples from 471 participants in the Osteoarthritis Initiative (OAI) (non-exposed reference control cohort, n = 98, and the FNIH OA Biomarkers Consortium cohort, n = 373) including 345 with radiographic knee OA (rKOA), defined as a Kellgren–Lawrence (KL) grade ≥2 in at least one knee. Synovitis was evaluated using two complementary features assessed by the MRI Osteoarthritis Knee Score (MOAKS): Hoffa-synovitis and effusion-synovitis, each graded from 0 to 3. Among participants with evaluable MRI data for each feature, Hoffa-synovitis was present in 163 of 307 (53%) participants, while effusion-synovitis was present in 125 of 296 (42%) **(Supplementary Figure 1).** Both features were present in 103 participants, whereas 122 had neither, highlighting that effusion-synovitis and Hoffa-synovitis represent complementary yet non-identical MRI-defined inflammatory features of the joint. Baseline characteristics stratified by MRI-defined synovitis phenotype are presented in **Table 1**. Hoffa-synovitis was associated with older age and male sex, whereas no differences in age or sex were observed for effusion-synovitis. Both MRI-defined features were associated with greater radiographic structural damage (higher KL grades), and greater knee pain, reflected by higher Western Ontario and McMaster Universities Osteoarthritis Index (WOMAC) pain scores and lower Knee injury and Osteoarthritis Outcome Score (KOOS) pain scores. Notably, patients with Hoffa-synovitis at baseline had an 83% higher risk of rKOA progression at 48 months after adjustment for age and sex (OR = 1.83, 95% CI 1.06–3.21) (**Supplementary Figure 2A**).

Metabolite-driven analyses were performed using 315 annotated plasma metabolites retained after preprocessing. To prioritize metabolites associated with synovitis, we performed exploratory partial least squares discriminant analysis (PLS-DA) separately for Hoffa-synovitis and effusion-synovitis (**Figure 1A**). Annotated metabolites with variable importance in projection (VIP) >1 and $p < 0.05$ were retained as candidate features, yielding 13 metabolites associated with Hoffa-synovitis and 6 metabolites associated with effusion-synovitis (**Figure 1B**). Free choline was the only metabolite shared between both candidate sets **(Figure 1C),** with VIP scores of 2.56 ($p = 0.0044$) for Hoffa-synovitis and 2.74 ($p = 0.0076$) for effusion-synovitis. Free choline was therefore prioritized as a nominated candidate from the discovery analysis and was

123 further confirmed by retention time and MS/MS matching against an authentic standard
124 (**Supplementary Figure 3**).

125 **Plasma choline tracks synovial inflammation rather than structural severity**

126 To determine whether circulating choline was associated with OA status or synovial
127 inflammation, we first compared participants with rKOA (n = 345) with individuals from
128 the OAI non-exposed reference control cohort (n = 98), who had no knee OA or major
129 risk factors for developing the disease. Plasma choline abundance did not differ between
130 groups **(Figure 1D)**. Among participants with rKOA, choline abundance was higher in
131 those with either MRI-defined synovitis feature, with increased odds of Hoffa-synovitis
132 (OR 1.37, 95% CI 1.09–1.74; p = 0.0089) and effusion-synovitis (OR 1.40, 95% CI 1.10–
133 1.79; p = 0.0067). The strongest association was observed in participants with both
134 features compared with those with neither (OR 1.55, 95% CI 1.18–2.09; p = 0.0025)
135 **(Figure 1E)**. Consistent with these findings, each quartile increase in plasma choline
136 was associated with 31% higher odds of Hoffa-synovitis (OR 1.31, p-trend = 0.010) and
137 27% higher odds of effusion-synovitis (OR 1.27, p-trend = 0.025) **(Supplementary**
138 **Figure 2B)**.

139 Plasma choline was also positively associated with age, male sex, radiographic severity
140 (KL grade) and knee pain (higher WOMAC pain scores and lower KOOS pain scores)
141 **(Figure 1F)**. Importantly, higher plasma choline was associated with increasing MRI-
142 defined synovitis severity. After adjustment for age, sex and body mass index (Model 2),
143 each 1-SD increase in choline was associated with 29% higher odds of greater Hoffa-
144 synovitis severity (OR 1.29, 95% CI 1.03–1.61; p = 0.024) and 28% higher odds of
145 greater effusion-synovitis severity (OR 1.28, 95% CI 1.03–1.58; p = 0.025). Further
146 adjustment for baseline radiographic disease burden, assessed by the summed bilateral
147 KL grade (Model 3), did not materially change these associations (Hoffa-synovitis: OR
148 1.29, 95% CI 1.03–1.60; p = 0.026; effusion-synovitis: OR 1.28, 95% CI 1.03–1.58; p =
149 0.027) **(Figure 1G).**

150 **Circulating choline is associated with radiographic knee osteoarthritis**
151 **progression at 48 months**

152 We next investigated whether baseline circulating choline was associated with
153 radiographic OA progression over 48 months, defined as an increase of at least one
154 Kellgren–Lawrence (KL) grade in either knee. Participants who experienced radiographic
155 progression had higher baseline plasma choline abundance than non-progressors (p =
156 0.018) **(Figure 1H).** Each 1-SD increase in plasma choline was associated with 32%
157 higher odds of progression (OR 1.32, 95% CI 1.04–1.69; p = 0.026). This association

remained largely unchanged after adjustment for age, sex and body mass index (OR 1.33, 95% CI 1.03–1.72; p = 0.029), and further adjustment for baseline radiographic disease burden (OR 1.32, 95% CI 1.02–1.71; p = 0.038).

Given these associations, we explored whether circulating choline could partly account for the relationship between baseline Hoffa-synovitis and subsequent radiographic progression. Baseline Hoffa-synovitis was associated with a 14.3 percentage-point higher probability of rKOA progression at 48 months (total effect 0.143, 95% CI 0.052 to 0.232, p = 0.0016). Circulating choline accounted for 12.0% of this effect (proportion mediated, 95% CI 4.5 to 94.4, p = 0.010; average causal mediation effect [ACME] 0.017, 95% CI 0.004 to 0.040, p = 0.0088) (**Figure 1I**).

External cohort assessment and pooled analysis of circulating choline associations with synovitis

To further evaluate the association between circulating choline and synovitis, we examined the independent IMI-APPROACH cohort (n = 286), in which serum total choline was absolute quantified using an enzymatic assay. The external cohort consists of 220 women and 66 men, with no sex difference in serum total choline (p = 0.69; **Supplementary Figure 4A**). Among 274 participants with available radiographic data in the index knee, 109 had rKOA and 165 did not. Consistent with OAI, circulating choline did not differ according to rKOA status (p = 0.74) (**Supplementary Figure 4B**). Unlike OAI, MOAKS assessments were available only for the index knee in IMI-APPROACH cohort; therefore, synovitis in the contralateral knee could not be excluded in participants classified as having no synovitis and neither synovitis. Among participants with rKOA, effusion-synovitis was present in 32 (30%) and Hoffa-synovitis in 28 (26%), with 16 (15%) exhibiting both features and 64 (59%) neither.

in the index knee. Hoffa-synovitis was less frequent in IMI-APPROACH than in OAI (26% vs 47%), whereas the prevalence of effusion-synovitis was more comparable (30% vs 36%). IMI-APPROACH had a higher proportion of participants with isolated effusion-synovitis (15% vs 6%), while concomitant Hoffa- and effusion-synovitis was more frequent in OAI (30% vs 15%). Conversely, a greater proportion of participants in IMI-APPROACH had neither phenotype in the index knee (59% vs 35%). Adjusted estimates were consistently directionally associated with higher odds of synovitis, although none reached statistical significance. The strongest association was observed for Hoffa-synovitis where each 1-SD increase in choline was associated with 55% higher odds (OR 1.55, 95% CI 0.95–2.59; p = 0.085) (**Supplementary Figure 4C).** Serum choline concentrations according to synovitis status are shown in **Supplementary Figure 4D.**

Given the limited number of cases in the external IMI-APPROACH cohort, we combined estimates from OAI and IMI-APPROACH cohorts using harmonized single-knee definitions of synovitis and fixed-effect meta-analysis. Higher circulating choline was associated with Hoffa-synovitis (OR per 1-SD, 1.38, 95% CI 1.13–1.68; p = 0.001), effusion-synovitis (OR 1.31, 95% CI 1.07–1.60; p = 0.009), and the presence of both phenotypes versus neither (OR 1.48, 95% CI 1.16–1.88; p = 0.001). No between-cohort heterogeneity was observed for any outcome (I^2 = 0%). Importantly, associations in OAI remained unchanged when applying the harmonized single-knee definition instead of the original bilateral assessment **(Supplementary Figure 4E).**

A plasma metabolic signature of choline-rich foods is associated with circulating choline levels and synovitis severity

Choline is an essential dietary nutrient obtained through diet. To explore whether dietary exposure contributes to circulating choline levels, we used an untargeted plasma metabolomics-based approach to estimate individual food exposure from food-associated molecular signatures[16]. The MS/MS features from the OAI plasma samples were matched to the MS/MS library of foods, to obtain food scores that estimate dietary exposure, for each participant, per each food category[17]. This approach provided a plasma-based measure of food exposure that was independent of self-reported questionnaire of dietary intake. We then constructed a choline rich food score by combining the signals from 8 animal source foods with a high choline content: egg, meat (beef, veal, pork), poultry, and seafood (salmon, langostino and tilapia) (**Figure 2A**). The resulting choline-rich food score showed a positive correlation with circulating free choline levels (Spearman ρ = 0.32, p < 0.001) (**Figure 2B**), which remained significant after adjustment for age, sex, BMI and baseline KL (p < 0.001). In contrast, a low-choline food score derived from foods with lower choline content, including fruit, grains, seeds, vegetables, and fungi was unrelated to circulating choline (ρ = 0.007, p = 0.88) (**Figure 2C**). This contrast is important because it indicates that the association is not simply driven by overall food-related metabolic signals. Instead, the plasma metabolomics signatures capture foods expected to contribute more strongly to choline availability. Having established that the choline-rich food signature correlates with circulating choline, we next investigated whether this signature was also associated with synovial inflammation in participants with rKOA.

The choline-rich food score was higher in participants with synovitis across all MRI-defined features (all p < 0.001) (**Figure 2D**). These associations persisted after adjustment for age, sex, BMI and baseline radiographic disease burden (KL grade), with

each 1-SD increase in the score associated with 40% higher odds of Hoffa-synovitis (OR 1.40, 95% CI 1.11–1.75; p = 0.004) and 33% higher odds of effusion-synovitis (OR 1.33, 95% CI 1.06–1.67; p = 0.015). The strongest association was observed in participants with both features compared with neither, with 77% higher odds (OR 1.77, 95% CI 1.06–2.95; p = 0.030 (**Figure 2E**). The score did not predict radiographic KL progression at 48 months (OR = 1.10, 0.89–1.36, p = 0.38).

In sex-stratified analyses, the choline-rich food score was associated with greater synovitis severity in women. After adjustment for age, BMI and baseline KL grade, the score correlated with effusion-synovitis severity (ρ = 0.20, p = 0.002) and Hoffa-synovitis severity (ρ = 0.19, p = 0.004). Consistently, each 1-SD increase in the score was associated with 51% higher odds of greater effusion-synovitis severity (OR 1.51, 95% CI 1.16–1.95) and 34% higher odds of greater Hoffa-synovitis severity (OR 1.34, 95% CI 1.03–1.75). No statistically significant associations were observed in men (effusion-synovitis: ρ = −0.09, p = 0.27; OR 0.81, 95% CI 0.62–1.06 **(Figure 2F and Supplementary Figure 5**).

Synovial choline is associated with synovial inflammation

The association of circulating choline with synovitis raised the question of whether choline metabolism is active within the OA joint. To investigate the cellular distribution of choline-handling machinery, we analyzed publicly available single-cell RNA-sequencing data from human OA synovial tissue (n = 9), focusing on choline transporters and choline kinase α (*CHKA*), the enzyme responsible for phosphorylating choline to phosphocholine (**Figure 3A**). *CHKA* expression was detected predominantly in myeloid and stromal cells, while *SLC44A1*, encoding the choline transporter CTL1, was the most highly expressed SLC44-family member in the stromal compartment (**Figure 3B**). Given this expression pattern and the central role of fibroblast-like synoviocytes (FLS) as a major resident cell population of the synovium, we focused subsequent analyses on the stromal compartment. Among 2,925 stromal cells, *SLC44A1* was detected in 1,656 (56.6%), *CHKA* in 542 (18.5%), and both genes in 346 (11.8%). *SLC44A1* expression was broadly distributed across synovial fibroblast populations, whereas *CHKA* was preferentially detected in lining fibroblasts, including 26.5% of *CLIC5*$^{+}$ and 22.6% of *VCAM1*$^{+}$ lining fibroblasts, compared with 13.4% of sublining fibroblasts (**Supplementary Figure 6A**). To further explore their metabolic potential, FLS were classified as *SLC44A1*-only, *CHKA*-only, double-positive or double-negative based on detectable expression of both genes**.** Notably, double-positive FLS showed enrichment of phosphatidylcholine

metabolism-related pathways **(Figure 3C),** suggesting that these cells possess the molecular machinery for choline uptake and metabolism.

To validate these findings at protein level, we examined synovial tissue from patients with end-stage OA. Dual immunofluorescence colocalized choline transporter-like protein 1 (CTL1), with vimentin-positive cells, a mesenchymal marker commonly expressed by FLS **(Figure 3D and Supplementary Figure 6B**). ChoKα was also detected in vimentin-positive cells (**Supplementary Figure 6C**) supporting the presence of choline uptake and phosphorylation machinery in OA synovial fibroblasts. We next examined whether metabolites of the choline metabolic pathway were associated with synovial inflammation. We quantified free choline, phosphocholine (PCho) and glycerophosphocholine (GPC) in human OA synovial tissue by proton nuclear magnetic resonance (^{1}H-NMR) spectroscopy, with representative spectra shown in **Supplementary Figure 6D.** Choline and PCho were positively associated with Krenn lining inflammation and vimentin staining. Choline also correlated with lining CD68 staining. Increasing vimentin staining was associated with lower GPC/choline and GPC/PCho ratios but a higher PCho/GPC ratio suggesting a shift toward choline phosphorylation and pathway activation in fibroblast-rich synovium (**Figure 3E**).

Choline availability promotes inflammatory and migratory responses in fibroblast-like synoviocytes

To determine whether extracellular choline availability directly influences intracellular choline levels, we measured the uptake of the stable-isotope tracer choline-d9 in primary human FLS. Choline-d9 was detected intracellularly within 10 min, with uptake increasing in response to higher extracellular choline concentrations ($p = 0.0046$) **(Figure 3F).** We then examined whether increased choline availability altered FLS function. Choline supplementation (3.5–20 μM) dose-dependently increased IL-8 and IL-6 secretion ($p = 0.011$ and $p = 0.00068$, respectively) and FLS migration ($p = 0.0015$). At 20 μM, IL-8 secretion increased 5.3-fold (95% CI 1.9–14.9) and IL-6 secretion 2.9-fold (95% CI 2.7–3.1) compared with 3.5 μM basal levels (**Figure 3G**), and wound width was 0.57-fold that observed at 3.5 μM (95% CI 0.46–0.71) (**Figure 3H**). Exact permutation tests within cell lines further supported dose-dependent changes in cytokine secretion and migration ($p = 0.00013$ for both cytokines; $p = 0.00026$ for migration).

ChoKα inhibition attenuates pathogenic fibroblast behavior and fibroblast-like synoviocytes-driven cartilage catabolism in vitro

Having shown that increased choline availability promotes inflammatory and migratory responses in FLS, we investigated whether inhibiting choline phosphorylation could suppress their pathogenic behavior. We used MN58b, a selective competitive inhibitor of choline kinase α (ChoKα) previously shown to inhibit its activity in FLS[18]. MN58b treatment (5 µM, 24 h) did not affect FLS viability (**Figure 4A**). We inhibited ChoKα in human OA synovial explants (n =4) and FLS (n =3) under basal and TNF stimulated conditions. In both synovial explants (**Figure 4B**) and FLS (**Figure 4C**), MN58b significantly reduced TNF-induced secretion of IL-6, MMP-3 and MMP-13 (all $p < 0.001$). Beyond inflammatory mediator release, ChoKα inhibition also impaired key pathogenic properties of FLS. MN58b significantly reduced FLS proliferation under TNF-stimulated conditions, as assessed by EdU incorporation ($p < 0.001$; **Figure 4D**), and decreased their migratory ($p = 0.006$; **Figure 4E**) and invasive capacity ($p = 0.013$; **Figure 4F**).

We next explored whether reducing FLS aggressiveness through ChoKα inhibition could limit structural joint damage by attenuating cartilage degradation. To investigate this, we stimulated FLS with TNF to induce an inflammatory phenotype, with and without the ChoKα inhibitor MN58b, and transferred their conditioned media to primary chondrocytes isolated from the same donors (n=5). Conditioned medium from MN58b-treated FLS induced significantly less nitrite release by chondrocytes than medium from FLS stimulated with TNF alone ($p < 0.001$) **(Figure 4G),** suggesting that ChoKα inhibition reduces the pro-inflammatory effects of FLS on cartilage cells. Notably, in human cartilage explants MN58b also reduced TNF-induced release of nitric oxide (NO), MMP-3, and MMP-13 (all $p < 0.0001$) (**Figure 4H**). Under IL-1β stimulation, MN58b also reduced NO ($p = 0.014$) and glycosaminoglycan (GAG) ($p = 0.02$) release (**Figure 4I**), consistent with a direct chondroprotective effect.

ChoKα inhibition attenuates synovitis and structural joint damage in vivo

To evaluate the in vivo effects of pharmacological ChoKα inhibition, MN58b was tested in two complementary murine models of OA: the collagenase-induced OA (CIOA) model (**Figure 5A**), characterized by synovial inflammation, and the destabilization of the medial meniscus (DMM) model (**Figure 5B**), a surgically induced OA model characterized primarily by cartilage and bone damage.

In the CIOA model, ChoKα inhibition significantly reduced synovial thickening, as reflected by a lower synovitis score compared with vehicle-treated mice (1.8 ± 1.60 vs 0.25 ± 0.71; **Figure 5C**). Immunohistochemical (IHC) analysis showed increased ChoKα expression throughout the synovium lining of CIOA control mice, whereas MN58b treatment markedly reduced ChoKα staining. Increased staining for the macrophage

markers iNOS and CD68 further confirmed the inflammatory phenotype of the CIOA model. MN58b reduced both iNOS and CD68 staining, indicating decreased macrophage-associated synovial inflammation (**Figure 5D**). Together, these findings demonstrate that ChoKα inhibition attenuates synovitis in the CIOA model.

The effect of MN58b on structural joint damage was subsequently evaluated in the non-inflammatory, surgical destabilization of the medial meniscus (DMM) model. Cartilage damage was assessed in Safranin O-stained sections using the OARSI scoring system. MN58b-treated mice showed less severe cartilage damage in both the medial and lateral compartments **(Figure 5E).** Bone changes were evaluated by Mmcro-computed tomography (μCT) (**Figure 5F**). While medial osteophyte size was lower in MN58b-treated mice based on histological assessment, although the difference was not statistically significant (1.04 ± 0.59 vs 0.72 ± 0.60; p = 0.10), μCT showed a 28% reduction in medial osteophyte size with MN58b treatment (p = 0.041) **(Supplementary Table 1)**.

DISCUSSION

Osteoarthritis (OA) is a highly prevalent and heterogeneous disease and a leading cause of chronic pain and disability worldwide, yet no established treatments can slow or prevent its progression[19, 20]. Synovitis, the inflammation of the joint's synovial membrane, is increasingly recognized as a key determinant of OA, contributing to pain and being associated with disease onset and structural progression[5, 10]. Understanding the biological mechanisms driving synovial inflammation is therefore essential to better characterize inflammatory OA, unravel the mechanisms contributing to disease heterogeneity, and identify new therapeutic opportunities. Here, we identify choline metabolism as a potentially targetable pathway linking systemic metabolic alterations to synovial inflammation in patients with radiographic knee OA (rKOA). Through untargeted plasma metabolomics, we identified free choline as a circulating metabolite associated with two MRI-defined features of synovitis: effusion-synovitis and Hoffa-synovitis. Circulating choline tracked synovitis severity independently of baseline radiographic severity and was associated with structural progression over 48 months. Importantly, we extended these clinical observations to human synovial tissue and experimental models, demonstrating that choline availability promotes inflammatory fibroblast responses, whereas pharmacological inhibition of ChoKα attenuates synovial inflammation and structural joint pathology.

Our findings extend the association between circulating choline and synovitis to the joint itself, supporting a role for local choline metabolism in OA inflammation. The expression of choline transport and phosphorylation machinery in synovial fibroblasts, together with tissue metabolite profiles associated with histological inflammation, provides biological support for this connection. Previous studies have implicated choline metabolism in macrophage activation, where inflammatory stimulation enhances choline uptake and phosphatidylcholine synthesis[21, 22]. ChoKα has also been implicated in rheumatoid arthritis fibroblasts, where its inhibition reduces pathogenic cell behavior and experimental inflammatory arthritis[18]. In OA synovial fibroblasts, we demonstrate that extracellular choline availability influences inflammatory and migratory responses, whereas ChoKα inhibition attenuates their pathogenic behavior. The convergence of these observations supports choline metabolism as a functional contributor to synovial inflammation rather than merely a circulating marker.

The association between circulating choline and subsequent radiographic progression raises the possibility that choline metabolism contributes to structural joint pathology in OA. Exploratory mediation analysis further suggested a potential contribution of circulating choline to the association between Hoffa-synovitis and progression, although causality cannot be established from these observational data. Supporting a possible link between synovial inflammation and cartilage pathology, ChoKα inhibition in FLS reduced the inflammatory response of chondrocytes exposed to their conditioned medium. In vivo, pharmacological inhibition attenuated synovial inflammation in the collagenase-induced OA model and reduced cartilage and bone pathology in the destabilization of the medial meniscus model. These findings suggest that choline metabolism may influence processes contributing to structural joint damage, potentially through inflammatory interactions between the synovium and cartilage.

Diet represents a potentially modifiable systemic factor in OA, yet whether it contributes to synovial inflammation and through which metabolic pathways remain poorly understood. Previous studies in the Osteoarthritis Initiative have linked dietary patterns, overall diet quality and specific nutrients to OA radiographic incidence[23-25], progression[26-29], and symptoms[30-32]. However, to our knowledge, none of these studies have examined the relationship between diet and synovitis in OA. Moreover, most of these studies have primarily relied on dietary questionnaires, which capture patterns of intake but do not directly reflect the biologically active metabolites through which diet may influence disease processes. The association of a choline-rich food signature with both circulating choline and synovitis suggests a potential link between dietary exposure and synovial inflammation in OA. Choline is an essential nutrient involved in membrane biosynthesis

and cellular signaling[33] and controlled feeding studies have demonstrated that circulating choline responds to dietary availability[34]. While humans can synthesize some choline de novo, most is obtained from diet. Nevertheless, circulating choline also reflects endogenous phospholipid metabolism and tissue uptake[33], and we cannot exclude the possibility that these factors contribute to the inflammatory phenotype of the joint. Although these findings do not establish a causal role for dietary choline in synovitis, our functional experiments demonstrate that choline availability directly influences inflammatory responses in synovial fibroblasts, providing biological support for this association and a rationale for future dietary intervention studies.

Synovitis has been extensively studied at the molecular level in joint tissue[35], yet few studies have identified circulating biomarkers of synovial inflammation in OA. In women, targeted studies linked serum MMP-3 to MRI-quantified effusion-synovitis in early OA[36] and identified cystine, uric acid, and tyrosine as metabolites associated with both OA severity and effusion-synovitis[37]. More recently, bile acids were associated with high-grade synovitis in a small exploratory cohort[38]. We extend this evidence by identifying a circulating metabolite linked to synovitis severity and subsequent structural progression, supported by functional experiments targeting the same metabolic pathway. Notably, circulating free choline was higher in men, whereas associations between the choline-rich food signature and synovitis severity were predominantly observed in women. Sex-dependent choline metabolism may contribute to these patterns, as endogenous phosphatidylcholine synthesis through PEMT is estrogen-responsive and choline requirements differ according to hormonal status[39]. Previous studies in the OAI cohort have also linked ultra-processed food consumption to worse knee OA outcomes, with stronger associations in women[40]. These observations warrant further investigation, particularly to determine whether sex modifies the relationship between dietary choline exposure and synovial inflammation.

Several limitations should be considered. Effusion- and Hoffa-synovitis were assessed by non-contrast MRI and represent surrogate measures of synovial inflammation rather than direct assessment of synovial enhancement. Although associations in the independent IMI-APPROACH cohort were directionally consistent with those in OAI, they did not reach statistical significance individually, and the pooled estimates were predominantly informed by OAI. Importantly, choline measurements differed between cohorts: OAI quantified the relative abundance of free choline in plasma using untargeted LC–MS/MS, whereas IMI-APPROACH measured absolute concentrations of total choline in serum using an enzymatic assay, encompassing free choline, phosphocholine and glycerophosphocholine. Free choline nevertheless represents the largest fraction of

this pool[41]. Synovitis assessment also differed between cohorts: OAI used bilateral MRI, whereas IMI-APPROACH assessed only the index knee. Therefore, synovitis in the contralateral knee could not be excluded among participants classified as unaffected in IMI-APPROACH. The external cohort also had a lower prevalence of radiographic knee OA and synovitis, with a higher proportion of participants presenting isolated effusion-synovitis. Together with the smaller number of synovitis cases, these differences limited the precision and comparability of the external estimates. In addition, the observational associations, including the mediation analysis and dietary findings, cannot establish causality. Human tissue and functional studies primarily involved patients with end-stage OA, limiting generalizability to earlier disease stages. Finally, pharmacological inhibition does not establish that ChoKα mediates all effects of extracellular choline, and systemic MN58b administration prevents attribution of the in vivo effects to a specific joint cell population.

In conclusion, our study identifies choline metabolism as a therapeutically tractable pathway associated with inflammation-driven OA, advancing the biological characterization of a clinically important inflammatory component of this heterogeneous disease. By connecting circulating metabolic alterations with local synovial mechanisms and experimental intervention, our findings provide a rationale for investigating ChoKα inhibition as a strategy to reduce joint inflammation and potentially slow structural progression. The association between dietary metabolic signatures and synovitis further opens the possibility of exploring nutritional interventions as a complementary approach. Whether targeting choline metabolism can alter the course of OA in patients remains to be established.

METHODS

Discovery cohort: Participants**.** We conducted a baseline cross-sectional analysis of plasma samples from participants in the Osteoarthritis Initiative (OAI)[42] The analysis included individuals from the OAI non-exposed reference control cohort (n = 98), which comprises participants without knee symptoms, radiographic tibiofemoral OA, or major OA risk factors, and participants from the FNIH OA Biomarkers Consortium cohort (n = 373), a nested case-control cohort within the OAI selected to study biomarkers of structural and symptomatic knee OA progression. Details of the study design had been previously published[43, 44]. Participants from the FNIH cohort without radiographic knee osteoarthritis (rKOA), defined as Kellgren–Lawrence (KL) grade < 2 bilaterally at

baseline, were excluded (n = 28), leaving 345 participants with rKOA eligible for synovitis assessment.

MRI and imaging outcomes**.** Synovitis was evaluated at baseline in patients with rKOA on non-contrast MRI using two independent measures: effusion-synovitis and Hoffa-synovitis, each scored from 0 to 3 in both knees according to the MRI Osteoarthritis Knee Score (MOAKS)[45, 46]. Hoffa-synovitis is a term used for signal changes in Hoffa's fat pad that are commonly used as a surrogate for synovitis on non-contrast-enhanced MRI. For each MRI-based measure, the presence of synovitis was defined as a score ≥2 in at least one knee, whereas absence of synovitis was defined as bilateral scores <2. Synovitis severity was defined as the summed bilateral MOAKS score (range 0–6) and was restricted to participants with available bilateral MRI and scoring available. The Hoffa-synovitis analysis included 307 participants; 163 participants met the criteria for Hoffa-synovitis and 144 did not. The effusion-synovitis analysis included 296 participants; 125 participants had effusion-synovitis and 171 did not (**Supplementary Figure 1).** Among participants with rKOA and bilateral available baseline KL grades available, structural burden was calculated as the summed KL grade across both knees (range 0–8). KL progression was defined as an increase of ≥1 KL grade from baseline to 48 months in at least one eligible knee, excluding knees with baseline KL grade 4; non-progressor status required no KL progression in both eligible knees. MRI assessment in the OAI cohort: The osteoarthritis initiative 3 Tesla MRI knee protocol includes the following sequences: coronal intermediate-weighted (1) 2D turbo spin-echo (TSE), sagittal 3D dual-echo in steady state (DESS) with water excitation that can be reformatted on the coronal and axial planes, coronal T1-weighted 3D fast low-angle shot (FLASH), sagittal IW 2D TSE fat-saturated, and sagittal 2D multi-echo spin-echo (MESE). Sagittal intermediate-weighted fat-suppressed turbo spin echo (TR/TE, 3200/30 ms; FA = 180°) and axial reformatted water-excitation dual-echo in steady state (TR/TE, 16.3/4.7 ms; FA = 25°) sequences were also used in this study. Effusion-synovitis and Hoffa-synovitis at baseline were graded by a fellowship-trained musculoskeletal radiologist, blinded to the subject clinical information, according to the MRI Osteoarthritis Knee Score (MOAKS)[45, 46]. Effusion-synovitis was reported as high signal intensity (fluid-equivalent) within the joint cavity on the axial reformatted 3D DESS WE MR sequence excluding periarticular cysts and ganglia: Grade 0 = none (physiological), grade 1 = small (fluid continuous in the retropatellar space), grade 2 = medium (slight convexity of the suprapatellar bursa) and grade 3 = large (evidence of capsular distension). Hoffa-synovitis was reported as diffuse high-signal intensity within the fat pad on the mid-slices of the sagittal IW 2D TSE fat-saturated MR sequence. The score was based on size: 0

= normal, 1 = mild, 2 = moderate, 3 = severe. All images were analyzed using Osirix DICOM Viewer[47].

External cohort:

Population and imaging outcomes. IMI-APPROACH (Innovative Medicines Initiative—Applied Public–Private Research enabling OsteoArthritis Clinical Headway, https://www.approachproject.eu) is an observational, longitudinal study that enrolled 297 OA patients at five clinical centers in Europe[48]. Participants were recruited from five existing observational cohorts: CHECK in Utrecht, the Netherlands; HOSTAS in Leiden, the Netherlands; MUST in Oslo, Norway; PROCOAC in A Coruña, Spain; and DIGICOD in Paris, France. IMI-APPROACH was conducted in accordance with Good Clinical Practice, the Declaration of Helsinki and the applicable ethical and regulatory requirements at each participating center. All participants provided written informed consent, and the study was registered at ClinicalTrials.gov under identifier NCT03883568. MRI of the index knee was acquired at five clinical centers using harmonized 1.5-T or 3-T protocols suitable for semiquantitative assessment, as described previously[49].

The external evaluation included 286 participants with available baseline serum and corresponding clinical and radiographic data, of whom 109 had rKOA, defined as a Kellgren–Lawrence grade ≥2 in the predefined index knee. Effusion-synovitis and Hoffa-synovitis were evaluated on baseline non-contrast MRI of the index knee using MOAKS and scored from 0 to 3. Each feature was considered present when the score was ≥2 and absent when the score was <2, although classification in IMI-APPROACH was based on the index knee rather than bilateral MRI. Among the 109 participants with rKOA, 32 had effusion-synovitis and 77 did not. Hoffa-synovitis data were available for 107 participants, of whom 28 had Hoffa-synovitis and 79 did not. Sixteen patients had both synovitis phenotypes, whereas 64 had neither. Circulating total choline was quantified in baseline serum using an enzymatic assay (Choline Assay Kit, Abcam, ab219944), according to the manufacturer's instructions. In this assay, total choline comprises water-soluble quaternary ammonium compounds, including phosphocholine, glycerophosphocholine, and free choline. To validate the relative MS/MS measurements of free choline in the OAI cohort, we additionally quantified free choline in a subset of 60 OAI serum samples selected to span the observed MS/MS measurement range, comprising the 30 samples with the highest and 30 with the lowest relative MS/MS free choline abundances. Relative MS/MS free choline abundance correlated with enzymatic assay-based quantification (Spearman's $\rho = 0.745$, $p < 0.001$).

Sample preparation for LC-MS analyses: Initially, a 96 well plate Phree Kit was put on the top of a 96 deep well plate, and 40 µL of blood plasma was transferred to a 96 well plate Phree Kit for phospholipid removal. 160 µL of 100% methanol was added to the serum sample and mixed gently pipetting up and down five times. The plates were then centrifuged for 5 min at 1,300 g to yield the filtered blood serum samples. The samples were dried on a CentriVap (Labconco) and stored at -80 °C until LC-MS analyses. The samples were resuspended in 80 µL 50:50 methanol/water containing 1 µM sulfadimethoxine as an internal standard before LC-MS analyses.

Untargeted LC-MS/MS data acquisition: The LC-MS/MS analyses were performed with a Vanquish UHPLC system coupled to a Q-Exactive Orbitrap mass spectrometer (Thermo Fisher Scientific). The chromatographic separation was performed with a C18 porous core column (Kinetex C18, 50 x 2.1 mm, 1.7 µm particle size, 100 A pore size – Phenomenex, Torrance, USA), and the mobile phase consisted of solvent A as H2O, and solvent B as acetonitrile (ACN) – both containing 0.1 % formic acid (FA). The gradient employed was: 0-1 min isocratic at 5% B and 1-7 min from 5% B to 100% B as linear gradient, followed by column washing for 2.5 min, and another 1.5 min for re-equilibration at 5% B. The flow rate was set as 0.5 mL/min, injection volume as 3 µL, and column temperature of 40 ˚C. The tandem mass spectra were acquired using Data-Dependent Acquisition (DDA) mode in positive ionization mode. The parameters for the electrospray ionization (ESI) were set as follows: 60 AU sheath gas flow, 20 AU auxiliary gas flow, 3 AU sweep gas flow, and 300 °C auxiliary gas temperature; the spray voltage was set to 3.5 kV and the inlet capillary to 380 °C and 60 V S-lens level was applied. MS scan range 100-1500 m/z with a resolution of 35,000, and MS/MS scan range starting at 50 m/z with a resolution of 17,500 was applied. The maximum ion injection time for MS/MS scans was set to 100 ms, with an AGC target of 5E5 ions. The MS/MS precursor isolation window was set to 1.5 m/z. The normalized collision energy was set to a stepwise increase from 20 to 30 to 40%. MS/MS scans were triggered at the apex of the chromatographic peaks within 2 to 8 s from their first occurrence. Dynamic precursor exclusion was set to 10 s.

MS/MS data processing: The acquired raw LC-MS/MS data were converted to mzML format using MSConvert (ProteoWizard, Palo Alto, CA, USA)[50], and the data was processed using MZmine4[51] version 4.0.8. The mzML files were imported using the advanced import module with both MS1 and MS2 detection set to centroid, with a noise level set to 5.0E4 for MS1, and to 3.0E3 for MS2. The chromatogram construction was performed, where the minimum consecutive scan was set to 3, the minimum intensity for consecutive scans was set to 1.0E4, minimum absolute height set to 5.0E3, and

tolerance set to 0.01 m/z or 10 ppm. A smoothing of the chromatograms was applied using Savitsky Golay algorithm, with retention time (RT) smoothing set to 5. The local minimum feature resolver module was used for chromatogram deconvolution, with a chromatographic threshold of 90%, a minimum search range in RT of 0.2 min, a minimum relative height of 1%, minimum absolute height of 1.0E3, minimum ratio of peak top/edge of 2.0, a peak duration of 0.01-0.5 min, and a minimum of 3 data points. The 13C isotope filter module was used by setting an m/z tolerance of 0.01 m/z or 5 ppm, RT tolerance of 0.05 min, and setting the maximum charge to 2 and the representative isotope as the most intense one. Then, the features were aligned using tolerance of 0.01 m/z or 20 ppm, and RT tolerance of 0.2 min, giving a weight for m/z and RT as 3 and 1, respectively. Gap filling was then performed using an intensity tolerance of 20%, mass tolerance of 0.01 m/z or 20 ppm, RT tolerance of 0.2 min, and a minimum of 2 data points. A features list filter was applied to validate the 13C isotope pattern with a m/z tolerance of 0.0015 m/z to 5 ppm, with maximum charge of 2. Then, a duplicate peak filter was applied using new average filter mode with an m/z tolerance of 0.01 m/z or 20 ppm and an RT tolerance of 0.2 min. A peak area feature quantification table was exported as a .csv file, in addition to a consensus MS/MS spectral data in.mgf format. Raw peak areas were imported into R for statistical analysis. Features were filtered using blank controls by comparing mean intensities in blanks and biological samples; those with a sample-to-blank mean intensity ratio <5 were excluded. To account for the compositional structure and sparsity of untargeted metabolomics data, the filtered matrix was transformed using a robust centered log-ratio (rCLR) approach implemented in the *vegan* package. Features exhibiting near-zero variance were removed. All downstream analyses were conducted on rCLR-transformed intensities. Analyses were performed on the subset of annotated metabolites with matched compound identities in the MS/MS spectral libraries publicly available within the GNPS environment (https://pubmed.ncbi.nlm.nih.gov/27504778/). The analyses can be accessed at GNP2 (https://gnps2.org/status?task=61cf64b8247943248dbd6f9d83c3db14).

Data availability: Untargeted metabolomics data acquired is accessible using the MassIVE repository for both serum [dataset: MSV000095143]

Supervised multivariate discrimination and feature prioritization. Feature tables from untargeted metabolomics analyses were imported in R 4.5.0 (R Foundation for Statistical Computing, Vienna, Austria) for downstream data analyses. To explore whether the plasma metabolome differed by synovitis status, partial least squares discriminant analysis (PLS-DA) was performed using mixOmics package[52]. Separate PLS-DA models were generated for each MRI-defined synovitis outcome: effusion-

synovitis and Hoffa-synovitis. Variable importance in projection (VIP) scores were calculated, and annotated metabolites with VIP > 1 on component 1 were subsequently evaluated using Wilcoxon rank-sum tests comparing participants with and without synovitis. Candidate metabolites were prioritized based on concordant multivariate and univariate evidence, defined as VIP > 1 in the PLS-DA and nominal Wilcoxon $p < 0.05$. Candidate metabolites were identified independently for each synovitis outcome, and the final prioritized metabolites were defined as those consistently identified across both effusion-synovitis and Hoffa-synovitis analyses.

Statistical analysis. Group comparisons used two-sided Wilcoxon rank-sum or Kruskal–Wallis tests. The association between plasma choline and the presence of each synovitis phenotype was assessed by logistic regression across quartiles of choline, with linear trend tested over the quartile index. Synovitis severity was analyzed as an ordinal outcome to assess whether choline was associated with increasing MRI-defined inflammatory burden. Because few participants reached the maximum score of 6 (Hoffa, n = 9; effusion, n = 7), the highest categories were collapsed at ≥5. Proportional-odds ordinal logistic regression models were fitted to estimate the association between standardized choline relative abundance and increasing synovitis severity using the MASS package: choline alone (M1); choline adjusted for age, sex and BMI (M2); and choline further adjusted for summed baseline KL grade (M3). The proportional-odds assumption was tested by likelihood-ratio comparison of cumulative-link models with a common versus a threshold-specific choline effect (ordinal package). The proportional-odds assumption was evaluated for each synovitis phenotype. When this assumption was met, a single proportional-odds estimate was reported. When the assumption was rejected the overall association with choline was tested using a likelihood-ratio test from a model allowing threshold-specific choline effects. Threshold-specific odds ratios were also estimated at each cumulative cut-point, adjusted as in the fully adjusted model. Effect modification by sex was assessed using a likelihood-ratio test comparing ordinal models with and without a choline × sex interaction term. Additionally, to enable pooling of the OAI and external IMI-APPROACH cohorts, synovitis status was harmonized across cohorts. In OAI, synovitis was defined based on the most affected knee (MOAKS ≥2), whereas in IMI-APPROACH it was defined based on the index knee, for which MOAKS data were available. Per-1-SD log-odds ratios from both cohorts were then combined using inverse-variance fixed-effect meta-analysis (metafor). Between-cohort heterogeneity was assessed using I^2.

Mediation analysis. Mediation analyses were performed using the mediation package in R to assess whether candidate metabolites acted as intermediate variables linking

baseline MRI-defined synovitis to structural progression at 48 months. Effusion-synovitis and Hoffa-synovitis were modeled separately as exposures, and structural progression, defined as an increase of at least one Kellgren–Lawrence grade in either knee over 48 months, was modeled as the outcome. The mediator model estimated the effect of synovitis on metabolite levels using linear regression, and the outcome model assessed structural progression using logistic regression including both synovitis and the metabolite. Average causal mediation effects (ACME), average direct effects (ADE), total effects, and the proportion mediated were estimated using 5,000 quasi-Bayesian simulations[53]. To ensure directional consistency across the mediation pathway, analyses were retained only when the exposure–mediator, mediator–outcome, and total exposure–outcome coefficients were positive and consistent across the mediation components ($x_m_beta * m_y_beta * x_y_beta \geq 0$).

Plasma-derived dietary profiling using food metabolite signatures. To obtain an estimate of dietary exposure directly from plasma, we used a food-metabolite signature approach, which infers food-class exposure from the circulating metabolome. Applying a previously described LC–MS/MS food-reference framework[54], food-derived metabolites were matched against a curated food-metabolite reference library and aggregated, according to a hierarchical food ontology, into relative abundances for each food class ("food readouts"). Each participant thus received a quantitative, ontology-informed readout of diet-associated chemistry across multiple food classes and levels of resolution. Because these readouts derive from circulating metabolites rather than reported consumption, they capture the fraction of dietary food-class chemistry that reaches the plasma metabolome and are therefore complementary to, but distinct from, food-frequency data. Readouts were generated from the same plasma samples used for primary metabolomic analysis.

High- and low- choline food scores analysis. From the food readout (level-5 ontology), we constructed a high-choline score comprised eight animal-source foods selected a priori as rich in choline according to USDA FoodData Central[55]: egg, beef, veal, pork, poultry, salmon, langostino and tilapia; and a low-choline score from plant-source foods know to be low in choline (fruit, grain, seed, vegetables, fungi). Each food-class abundance was standardized (z-score) within the analytic sample. To prevent classes with more member-foods or larger magnitude from dominating the score, foods were first averaged within biological group (meat = beef/veal/pork; seafood = salmon/langostino/tilapia; egg; poultry) and the resulting group-level z-scores were then averaged; the score was re-standardized so that estimates correspond to a 1-SD increment. Foods included in each score were fixed a priori and were not selected based

on their association with outcomes. Associations between each score and synovitis severity were estimated with ordinal (proportional-odds) logistic regression, reporting the odds ratio per 1-SD increment together with Spearman correlations; the proportional-odds assumption was assessed for each model. For severity analyses, bilateral scores were summed for Hoffa-synovitis and effusion-synovitis separately (range, 0–6), with scores ≥5 collapsed into a single category, and jointly (range, 0–12), with scores ≥9 collapsed. Associations with the *presence* of synovitis were estimated with binary logistic regression. All models were adjusted for age, BMI and radiographic KL sum (and sex in pooled analyses). Effect modification by sex was tested by adding a score×sex interaction term (likelihood-ratio test against the nested model), followed by sex-stratified models. Outcomes were Hoffa-synovitis and effusion-synovitis (each summed bilaterally, 0–6, ≥5 collapsed), their combined sum (0–12, ≥9 collapsed).

Single-cell RNA-sequencing analysis of choline-pathway genes in OA synovium. Publicly available processed scRNA-seq data from the Accelerating Medicines Partnership Rheumatoid Arthritis/Systemic Lupus Erythematosus Phase 2 consortium were obtained from Synapse[56]. The original study included nine patients with OA. The processed dataset comprised 7,251 cells, including 2,925 cells annotated as stromal cells. Raw sequencing reads were not reprocessed, and the major cell-type and fine-grained cell-state annotations provided by the original study were retained. Cell-level quality control, doublet removal, batch correction and initial cell-state annotation were performed as described in the original study. Analyses were performed in Seurat using the RNA assay. The filtered count matrix was normalized using the LogNormalize method with a scale factor of 10,000. The 2,000 most variable genes were identified using variance-stabilizing transformation, and expression values were scaled across all genes. Principal-component analysis was performed using the variable genes. The OA subset was analyzed jointly without additional batch-correction or integration procedures.

Expression of *CHKA* and the *SLC44*-family choline transporters was examined across the major synovial cell compartments using normalized RNA expression. Dot plots were generated using Seurat, with dot size representing the percentage of cells with detectable expression and color representing scaled average expression. For fibroblast-focused analyses, cells annotated as stromal cells were classified according to detectable normalized expression (>0) of *SLC44A1* and *CHKA* as *SLC44A1*-only (n=1,310), *CHKA*-only (n=196), double-positive (n=346), or double-negative (n=1,073). These expression-defined groups were used for exploratory transcriptional characterization and were not considered discrete fibroblast subpopulations. Gene

Ontology enrichment analysis was performed using the gsfisher package. Gene symbols were mapped to Ensembl identifiers using the human annotation retrieved through biomaRt. Positively enriched genes identified by FindAllMarkers were tested using their multiple-testing-adjusted differential-expression P values, with all genes represented in the corresponding Seurat object and successfully mapped to Ensembl identifiers used as the background universe. Enrichment was evaluated across Gene Ontology Biological Process, Molecular Function and Cellular Component categories using Fisher's exact tests. Gene sets were filtered to retain terms containing at least three foreground genes and no more than 500 genes, with adjusted enrichment $P<0.05$ considered significant.

Human synovial tissue samples. Synovial tissue was obtained from patients with knee OA undergoing total joint-replacement surgery at the Veterans Affairs (VA) San Diego Health Care System. All participants provided written informed consent. The study protocol was approved by the VA Institutional Review Board (IRB H170130) and conducted in accordance with the Declaration of Helsinki. Surgical specimens were used, as detailed below, for histological and immunohistochemical analysis, ^{1}H-NMR metabolomics, isolation of fibroblast-like synoviocytes (FLS) and synovial explants.

Human articular cartilage explant and human primary chondrocyte isolation. Human articular cartilage explants were isolated from femoral condyle or tibial plateaus of surgical waste from total knee arthroplasty at the Veterans Affairs (VA) San Diego Health Care System. Cartilage was excised from macroscopically intact regions using a sterile scalpel. Uniform cylindrical explants (typically 3–8 mm diameter) were prepared using a biopsy punch, washed in PBS, and transferred to multi-well plates. Explants were equilibrated in culture medium - Dulbecco's modified Eagle's (DMEM) high glucose medium with 10% fetal calf serum (FCS), 100 μg/ml streptomycin, and 100 IU/ml penicillin at 37^0C for 24 hours before experiments. Human knee chondrocytes were isolated from articular cartilage obtained during total knee arthroplasty as described above. Cartilage was aseptically minced into small fragments and digested with collagenase type II (0.2% in culture medium) at 37 °C for 16 hours with gentle agitation. The resulting cell suspension was filtered through a 70-μm cell strainer, centrifuged, and resuspended in the same DMEM culture medium at 37^0C. No later than first passage chondrocytes were used.

Fibroblast-like synoviocytes (FLS) isolation and synovial explant culture. Primary FLS were isolated from OA synovial tissue obtained from patients undergoing joint replacement surgery for end-stage OA by enzymatic digestion and expanded in high-

glucose DMEM without pyruvate supplemented with 10% fetal bovine serum (FBS), L-glutamine (8 mM) and penicillin/streptomycin (100 U/mL) (Gibco, #15140122). For explant culture, OA synovial tissue was dissected into small pieces of comparable size and cultured in DMEM (Gibco, #11965092) supplemented with 10% FBS (Gibco #A56707-01).

Histological scoring and immunofluorescence analysis of OA synovial tissue. OA synovial tissue samples (n = 36) were fixed in 10% formalin (Thermo Scientific, #5735) and paraffin embedded. Sections (5 µm) were stained with hematoxylin and eosin (H&E), and synovitis severity was scored using the Krenn histopathological synovitis score including lining hyperplasia, sublining inflammation, and immune cell infiltration[57, 58]. Immunofluorescence (IF) was performed to assess CTL1 and vimentin colocalization, whereas immunohistochemistry (IHC) was used for vimentin and CD68 quantification, and ChoKα and vimentin colocalization. For IF, sections were deparaffinized, rehydrated, subjected to antigen retrieval in citrate buffer for 20 min, and treated to quench autofluorescence. Following blocking with 10% normal goat serum, sections were incubated overnight at 4 °C with antibodies against CTL1 (Proteintech 14687-1-AP) and vimentin (R&D Systems MAB2105-SP), followed by fluorophore-conjugated secondary antibodies, Hoechst counterstaining, and mounting with ProLong Gold. Images were acquired using a Zeiss AxioScan.Z1 (×20 objective). IHC was used to semi-quantitatively score macrophage (CD68 positive cells) and fibroblast (vimentin positive cells) presence in the ST samples, and for double-IHC with for ChoKα. IHC analysis was performed using 5 µM sections of formalin-fixed paraffin-embedded ST samples. After deparaffinization with xylene and rehydration with ethanol and water, antigen retrieval was performed by heating samples in citrate buffer pH 6 at 95 °C for 10 min with a pressure cooker. Next, endogenous peroxidase was inactivated with 3% H2O2 in water for 10 minutes at room temperature. Sections were then incubated with 3% bovine serum albumin (BSA) and 1% donkey serum in phosphate-buffered saline (PBS) for 1 hour at room temperature, and then with the specific primary antibody overnight at 4°C. Washing steps were performed with PBS and incubated with HRP or phosphatase alkaline-linked secondary antibody Impress system (Vector Labs, Burlingame, CA).The signal was developed using diaminobenzidine (brown color) for single IHC, or adding niquel (black color) (Vector Labs, Burlingame, CA) and Immpact™ Vector® Red (Vector Labs, Burlingame, CA) for double-IHC. Sections were lightly counterstained with hematoxylin, dehydrated with ethanol, cleared with xylene, and then mounted with a xylene-based medium. The antibodies and working concentrations used are listed as follows: CD68 (Abcam #ab955), Vimentin (Cell Signaling #D21H3), ChoKα (Proteintech #13520-I-AP).

The slides were scanned using a NanoZoomer or Olympus VS200 slide scanner using a 40x or 20x brightfield objective, respectively. Antibody expression was scored using a semi-quantitative scoring system from 0 to 3 in both the lining and sublining. The lining and sublining subscores were then summed to create a total expression score (maximum score of 6).

^{1}H-NMR metabolomics of synovial tissue. Metabolites in approximately 14 mg of synovial tissue (n = 36) were analyzed by proton nuclear magnetic resonance (^{1}H-NMR) spectroscopy. Spectra were acquired on a 600 MHz Bruker Avance III spectrometer, and metabolites were identified and quantified using Chenomx NMR Suite 8.5 Professional. Metabolite concentrations were normalized to tissue weight and reported in micromolar (µM).

Choline-d9 uptake assay. FLS were seeded in 6-well plates (1×10^5 cells/well) in complete medium (DMEM, 10% FBS) and cultured overnight. Cells were choline-starved for 3 h in choline-free medium (USBiological, #C5900-01), then incubated with choline-d9 chloride (Cayman Chemical, #36454) at 3.5, 10, and 20 µM for 10 min at 37 °C. Cells were washed three times with ice-cold PBS and lysed in 80% methanol. Lysates were collected, sonicated, centrifuged, dried by vacuum evaporation and analyzed by LC–MS/MS. Three wells were pooled per condition (3×10^5 cells/sample). A wash control (20 µM choline-d9, immediate washing without incubation) accounted for 1.1–1.4% of the signal after 10 min, indicating minimal extracellular tracer carryover. Values were normalized to the 3.5 µM condition for each donor (n= 3). The concentration-dependent trend was assessed using Page's trend test for ordered alternatives (one-sided).

Choline supplementation assays in FLS. To determine whether increased choline availability was sufficient to promote inflammatory and migratory FLS responses, primary FLS were cultured in choline-free medium (Usbio, #C5900-01) supplemented with 5% dialyzed FBS (dFBS) (Thermo #A3382001) and increasing concentrations of choline chloride (Thermo #110295000). Experiments were performed using samples from five biological donors (n = 5). For *cytokine secretion assays*, FLS were seeded in 96-well plates at 1,000 cells per well in triplicate for each condition in DMEM 10% FBS and allowed to adhere overnight. After one wash with PBS, cells were exposed to 5% dFBS choline-free medium supplemented with 3.5, 10, 20 or 100 µM choline chloride for 48 h. Then medium was replaced with fresh 5% dFBS choline-free medium containing the same choline concentrations, and cells were stimulated with TNF (20 ng/mL) (Peprotech #300-01) for 24 h. Supernatants were collected, and IL-6 and IL-8 were measure by ELISA according to the manufacturer’s instructions (R&D systems #DY206 and #DY208

respectively). *For migration assays*, FLS were seeded in 6-well plates at 100,000 cells per well and allowed to adhere overnight. Cells were then cultured for 48 h in choline-free medium supplemented with 5% dialyzed FBS and 3.5, 10, 20 or 100 µM choline chloride. A scratch wound was generated to create two cross-sections, after which wells were washed with PBS to remove detached cells and debris. Fresh choline-free medium supplemented with 5% dFBS and the corresponding choline concentration was then added, and cells were incubated for 48 h to assess migration. Cells were fixed with 4% paraformaldehyde for 30 min at 4 °C, washed with PBS, and stained with 0.05% crystal violet for 30 min at room temperature. Wells were washed three times with water and air-dried. Wound closure was quantified using ImageJ software[59]. Choline and cytokine concentrations were log10-transformed, and a linear regression was fitted across the three choline concentrations tested (3.5, 10, and 20 µM). Linear regression across the three choline concentrations (3.5, 10, and 20 µM) was used to estimate a dose–response slope for each cell line (n = 5). Slopes were tested against zero using a two-sided one-sample t-test, with an exact permutation trend test used as a sensitivity analysis

ChoKα inhibition in synovial explants and FLS. Explants and FLS were stimulated with human TNF 20ng/mL and treated with the ChoKα inhibitor MN58b (5 µM) or vehicle control for 24 hours. After treatment, culture supernatants were collected and *cytokine quantification* were quantified by enzyme-linked immunosorbent assays (ELISA) according to the manufacturer's instructions for human IL-6 (R&D systems # DY206), MMP-3 (R&D systems#DY513), and MMP-13 (R&D systems #DY511). *FLS viability* under ChoKα inhibition with MN58b was assessed by MTT assay. FLS were seeded at 2,000–3,000 cells per well in 96-well plates and starved overnight in 0.1% FBS. Then, conditions were applied in 1% and 10% FBS with MN58b (5 µM). On days 1 and 7, 20 µL of 10% 3-(4,5-dimethylthiazol-2-yl)-2,5-diphenyltetrazolium bromide (MTT) was added for 4 h at 37 C and dissolved in 200 µL DMSO. Optical density was measured at 550 and 690 nm for correction and averaged across replicates. *Proliferation* was assessed with the Click-iT Plus EdU Imaging Kit (Life Technologies) per the manufacturer's protocol. Glass coverslips were placed in 12-well plates and 15,000 FLS were seeded per well, starved overnight in 0.1% FBS, and treated the following day with conditions in 1% or 10% FBS ± MN58b (5 µM). Two days after adding conditions, EdU was added at 10 µM; two days later cells were fixed in 4% paraformaldehyde, counterstained with Hoechst (ThermoFisher #33342) and mounted. EdU-positive cells were counted from four random fields per coverslip acquired on a Keyence fluorescence microscope (×20; UCSD School of Medicine Microscopy Core). For *migration* assays, FLS were seeded at 150,000 cells per well in 6-well plates in 10% FBS overnight and

starved overnight in 0.1% FBS. Wells were scratched to create two cross-sections, washed with PBS, and treated with conditions ± MN58b (5 μM); cells were allowed to migrate for 24 h. Cells were fixed in 4% paraformaldehyde and stained with 0.05% crystal violet for 30 min, and migration across the wound margins was measured in ImageJ. *Cell invasion:* was assessed using spheroid outgrowth assay in Matrigel. FLS were grown to confluency, trypsinized and resuspended in ≈ 15 μL serum-free medium plus ≈ 15 μL Matrigel (Corning #356231). Two to three spheroids were formed per well in 12-well plates and allowed to set for 9 min, after which 1% or 10% FBS medium ± MN58b (5 μM) was added. After 24 h, spheroids were fixed in 4% paraformaldehyde, stained with crystal violet for 30 min, washed, and the invaded area surrounding each spheroid was photographed and quantified in ImageJ. *Nitric oxide (NO) assay:* NO release was measured as the concentration of nitrite in conditioned media by the Griess reaction, using $NaNO_2$ as standard. Experiments were performed using samples from five biological donors (n = 5).

In vivo validation. All mice were bred and maintained at the University of California, San Diego (UCSD) and handled in accordance with the guidelines of the UCSD Institutional Animal Care and Use Committee (IACUC), under approved protocols. Mice were kept on a 12 h light/dark cycle (light 06:00–18:00) at 68–72 °F with food and water ad libitum. All animal experiments were approved by the IACUC. Two mouse models were used to evaluate the in vivo effect of ChoKα inhibition: *collagenase-induced osteoarthritis (CIOA) and destabilization of the medial meniscus (DMM) models*. CIOA was induced in 12-week-old C57BL/6 mice (n = 17) by intra-articular injection of collagenase type VII (Sigma-Aldrich #C0773) on days 0 and 2. PBS or MN58b (2.5 mg/kg) was administered intraperitoneally (i.p.) starting 2 days before the intra-articular injection, with daily i.p. injections continued until sacrifice at 2 weeks. DMM was performed on the right knee of 12-week-old male C57BL/6 mice on day 0. PBS or MN58b (2.5 mg/kg) was administered i.p. every other day until sacrifice at 12 weeks post-surgery. Whole knee joints were harvested and fixed in Z-Fix for 72 hr at 4 °C. After an overnight PBS wash at 4 °C, micro-computed tomography (μCT) imaging in the joints from the DMM experiment was performed. *μCT*: μCT scans were translated, rotated, cropped and sliced for each femoral condyle (FC) and tibial plateau (TP) to visualize the medial and lateral FC (MFC, LFC) and TP (MTP, LTP) in a standardized orientation and field of view using custom semi-automated software (MATLAB). The FC and TP were positioned so their contact area was (1) at the physiological weight-bearing flexion angle of 60°, (2) aligned parallel to the horizontal, (3) rotated to a frontal view and (4) centered (Fang et al., Sci. Rep. 8:2855, 2018). Each region was visualized in tri-plane orthogonal

(frontal, sagittal, transverse) views and in periodic slices (every 0.05–0.075 mm transverse; every 0.075 mm frontal and sagittal), yielding 63 slices per femur and 78 per tibia (141 two-dimensional images per knee). Osteophytes were graded qualitatively (present/absent) and quantitatively (volume): periodic coronal and transverse/longitudinal slices were screened for irregular bone protruding outside the normal cortex (laterally from LFC/LTP; medially from MFC/MTP), each region scored 0 (normal) or 1 (osteophyte present); osteophyte volume in MFC and MTP was estimated from maximum dimensions in each orthogonal plane. Opposing osteophytes per compartment were graded 0 (none) or 1 (present in both MFC+MTP or LFC+LTP). *Histological Analysis of Synovitis and Cartilage Damage*: Knees were then decalcified for 72 h at room temperature on a shaker, washed overnight in PBS at 4 °C, dehydrated through 50% then 70% ethanol at 4 °C, and paraffin embedded. The entire joint was sectioned in the coronal plane at 5 µm. H&E-stained sections were used to score synovitis (0–3), including synovial thickening and inflammatory-cell infiltration. Safranin O–Fast, green-stained sections were used to score cartilage damage with the OARSI system, evaluating four quadrants per joint (medial tibial plateau (MTP), medial femoral condyle (MFC), lateral tibial plateau (LTP) and lateral femoral condyle (LFC)) with the average used for analysis; osteophyte size and maturity (0–3) and subchondral bone changes were also scored per OARSI. *Immunohistochemistry* was performed on 5-µm sections of formalin-fixed, paraffin-embedded knee joints from the CIOA experiment. Sections were deparaffinized, rehydrated through graded ethanol solutions, and subjected to heat-induced antigen retrieval in citrate buffer (pH 6.0) at 95°C for 30 min. Endogenous peroxidase activity was blocked with 3% hydrogen peroxide for 10 min, followed by incubation with 3% bovine serum albumin (Sigma Aldrich, #A7511-5G) in PBS (Fisher Scientific, #10010-023) for 1 h at room temperature. Sections were incubated overnight at 4°C with primary antibodies against ChoKα (Proteintech #13520-1-AP) and the macrophage marker CD68 (Abcam #ab955). After washing, the secondary antibody (anti-mouse and anti-rabbit ImmPRESS #MP-7402 andMP-7401) was incubated for 1 h at room temperature. Sections were lightly counterstained with hematoxylin, dehydrated, rehydrated. The slides were photographed slides using a Keyence microscope at 20x magnification.

Funding: M.G, P.C.D, and N.E.L are supported by NIAMS R21 AR082029 grant, R.P.G. is supported by Programa de axudas á etapa posdoutoral from Xunta de Galicia (IN606B-2024.22). V.C is supported by Instituto de Salud Carlos III (ISCIII), through the project RD24/0007/0026 and co-funded by the European Union. Microscopy imaging was performed at the UCSD School of Medicine Microscopy Core (NIH grants, NS047101, OD030505, OD036455)

Author contributions: R.P.G. processed the plasma samples, harmonized and curated the clinical databases, performed the metabolomics and statistical analyses, interpreted the results, performed the choline supplementation and choline-d9 experiments, and wrote the original draft of the manuscript. M.C. and R.C performed the ChoKα inhibition experiments in vitro and in vivo. A.F.L. and E.Y.C performed the MOAKS scoring. H.G. supported the food-omics analysis and performed retention-time matching for choline annotation. H.M.R. acquired and processed the LC-MS/MS plasma metabolomics data. V.C.L. implemented the computational pipeline for untargeted metabolomics analysis and acquired the mass spectrometry data for the choline-d9 tracing experiments. R.L. performed choline supplementation experiments. J.M.S. collected the synovial tissue samples and performed the ^{1}H-NMR analyses. M.S.C. performed the single-cell RNA-sequencing analysis. N.A. performed the histological scoring. Z.C. performed the immunofluorescence experiments. J.A. performed the quantification of the choline-d9 tracing experiments. S.A. contributed to NMR acquisition and processing. L.L. and V.C. performed the enzymatic quantification of choline in the IMI-APPROACH samples. A.C. collected the surgical synovial tissue. R.S. performed the μCT experiments and quantification. I.R., C.R.R. and F.J.B. contributed to the interpretation of patient characteristics and clinical classification. E.S.L. contributed to immunofluorescence studies and choline-related experiments. R.B. provided expertise in experimental OA models. N.E.L. contributed clinical expertise and contextualized the findings in OA. P.C.D. provided funding and metabolomics infrastructure for LC-MS/MS analyses. M.G. conceived and supervised the study and critically revised the manuscript. All authors reviewed, edited, and approved the final manuscript.

AI declaration statement: During the preparation of this manuscript, the authors used ChatGPT (OpenAI, GPT-5.6.]) for English language editing, condensation and readability, and Claude (Anthropic, Opus 5) for reviewing and cleaning analysis code. All AI-assisted text was reviewed, verified against the underlying data and results, and edited by the authors, who take full responsibility for the content of the manuscript.

967 **Table 1.** Baseline characteristics of study participants with radiographic knee osteoarthritis according to baseline Hoffa- and effusion-synovitis status. **NS**, not
968 significant; $p < 0.05$ (*), $p < 0.01$ (**), $p < 0.001$ (***). †Score calculated as the sum of the scores for both knees.

969

	Hoffa synovitis				Effusion-synovitis			
Variable	No (N=144)	Yes (N=163)	p-value	Significance	No (N=171)	Yes (N=125)	p-value	Significance
Age, years	60.69 (9.06)	63.15 (9.03)	0.018	*	61.58 (8.76)	62.19 (9.09)	0.561	NS
Female sex (n, %)	98 (68.1%)	82 (50.3%)	0.002	**	101 (59.1%)	73 (58.4%)	1	NS
Race (reference: Caucasian)	113 (78.5%)	119 (73.0%)	0.615	NS	133 (77.8%)	91 (72.8%)	0.217	NS
Body mass index (BMI), kg/m²	30.77 (4.92)	31.00 (4.75)	0.682	NS	30.58 (4.78)	31.51 (4.94)	0.104	NS
Kellgren–Lawrence grade †	3.78 (1.21)	4.62 (1.27)	<0.001	***	3.94 (1.24)	4.59 (1.31)	<0.001	***
Radiographic progression at 48months	27 (21.3%)	47 (33.1%)	0.04	*	33 (21.9%)	33 (30.8%)	0.113	NS
KOOS Symptoms score †	174.00 (24.86)	165.99 (24.31)	0.005	**	173.65 (24.20)	163.38 (25.07)	<0.001	**
KOOS Quality of Life score†	67.21 (21.63)	58.84 (21.02)	<0.001	***	67.16 (20.81)	56.32 (21.28)	<0.001	***
KOOS Pain score †	169.85 (30.24)	160.87 (30.06)	0.01	*	169.60 (29.70)	157.96 (30.83)	0.001	*
KOOS Sport and Recreation score†	71.01 (26.91)	63.95 (24.67)	0.045	*	71.09 (25.80)	61.28 (25.51)	0.008	**
WOMAC Stiffness score †	2.90 (2.66)	3.82 (2.69)	0.003	**	3.04 (2.65)	3.93 (2.76)	0.006	**
WOMAC Physical Function score †	16.23 (20.42)	21.85 (21.02)	0.018	*	16.34 (19.83)	23.64 (21.81)	0.003	**
WOMAC Pain score †	4.78 (5.74)	6.25 (5.89)	0.028	*	4.79 (5.68)	6.79 (6.03)	0.004	**
WOMAC Total score†	23.90 (27.96)	31.81 (28.06)	0.014	*	24.16 (27.06)	34.21 (29.16)	0.003	**

FIGURES

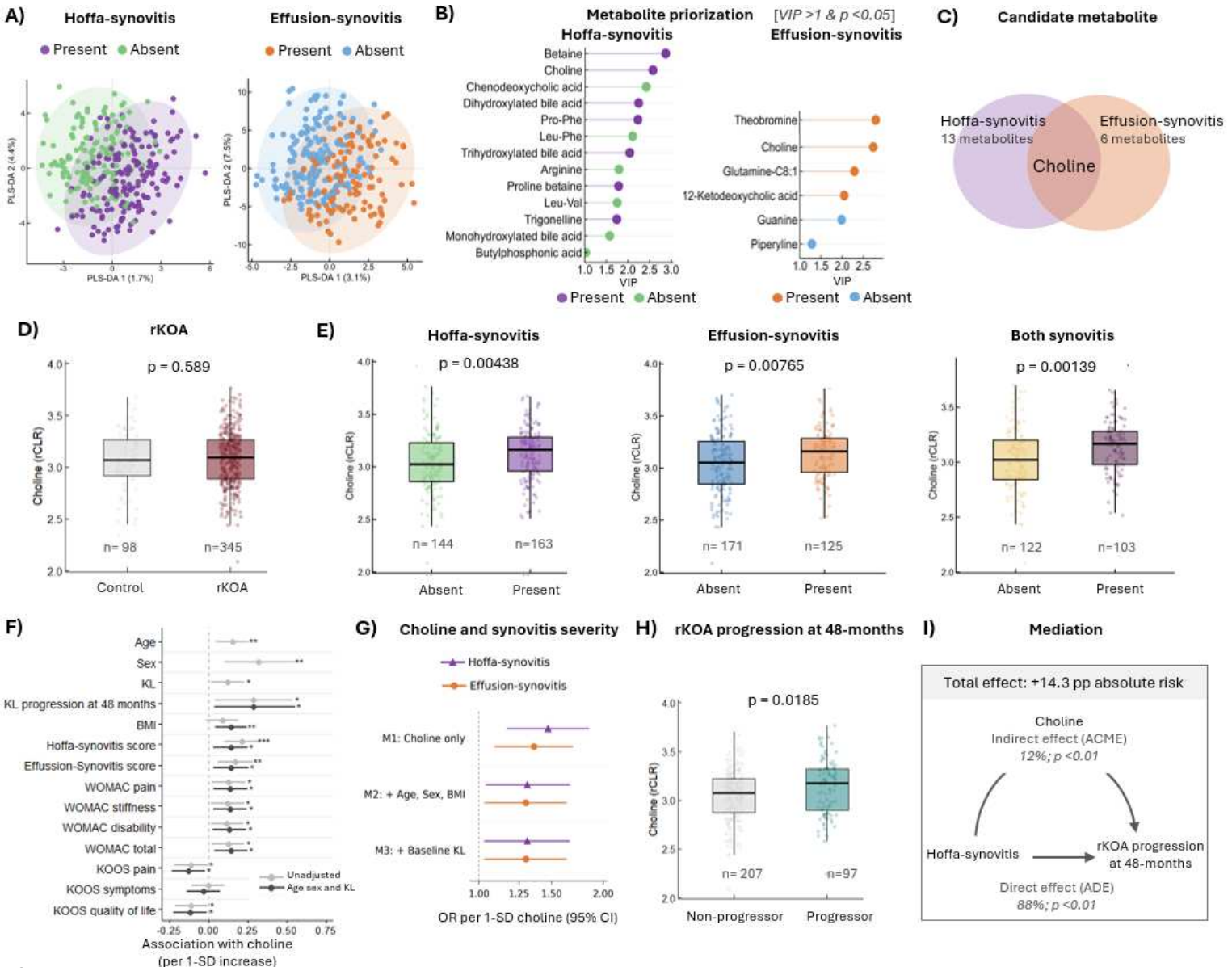


Figure 1 | Plasma free choline is associated with MRI-defined synovitis and 48-month radiographic progression in knee OA. (A) PLS-DA score plots of baseline rCLR-transformed plasma metabolomic profiles in participants with radiographic knee OA (rKOA), stratified by MRI-defined Hoffa-synovitis (n= 307) and effusion-synovitis (n=296). Ellipses, 95% confidence regions; axes show variance explained. (B) Annotated metabolites with VIP > 1 on component 1 and two-sided Wilcoxon P < 0.05; color indicates the group with higher relative abundance.Metabolite annotations were based on spectral matches against public MS/MS libraries and classified as level 2 according to the Metabolomics Standards Initiative. (C) Overlap of candidate metabolite lists from the two synovitis phenotypes. Free choline was the only shared metabolite and was confirmed at annotation level 1 by matching retention time and MS/MS spectra against an authentic standard. (D) Plasma choline in non-exposed reference controls (n = 98) and participants with rKOA (n = 345); two-sided Wilcoxon. (E) Plasma choline by Hoffa-, effusion- and combined synovitis status; two-sided Wilcoxon. (F) Associations of baseline plasma choline (per 1 SD) with clinical, structural and inflammatory variables, unadjusted (grey) and adjusted for age, sex and baseline KL (black); points, OR or β; bars, 95% CI. (G) Ordinal (proportional-odds) ORs per 1 SD choline for Hoffa- and effusion-synovitis severity. M1, unadjusted; M2, + age, sex, BMI; M3, + summed baseline KL. **(H)** Baseline plasma choline in participants with (n =97) and without KL progression (n=207) at 48 months; two-sided Wilcoxon. **(I)** Mediation analysis of the association between Hoffa-synovitis and 48-month radiographic KL progression through circulating choline. Indirect (ACME) and direct (ADE) effects were estimated using 5,000 quasi-Bayesian simulations. For box plots, center lines indicate medians, boxes the interquartile range, and whiskers 1.5× the interquartile range

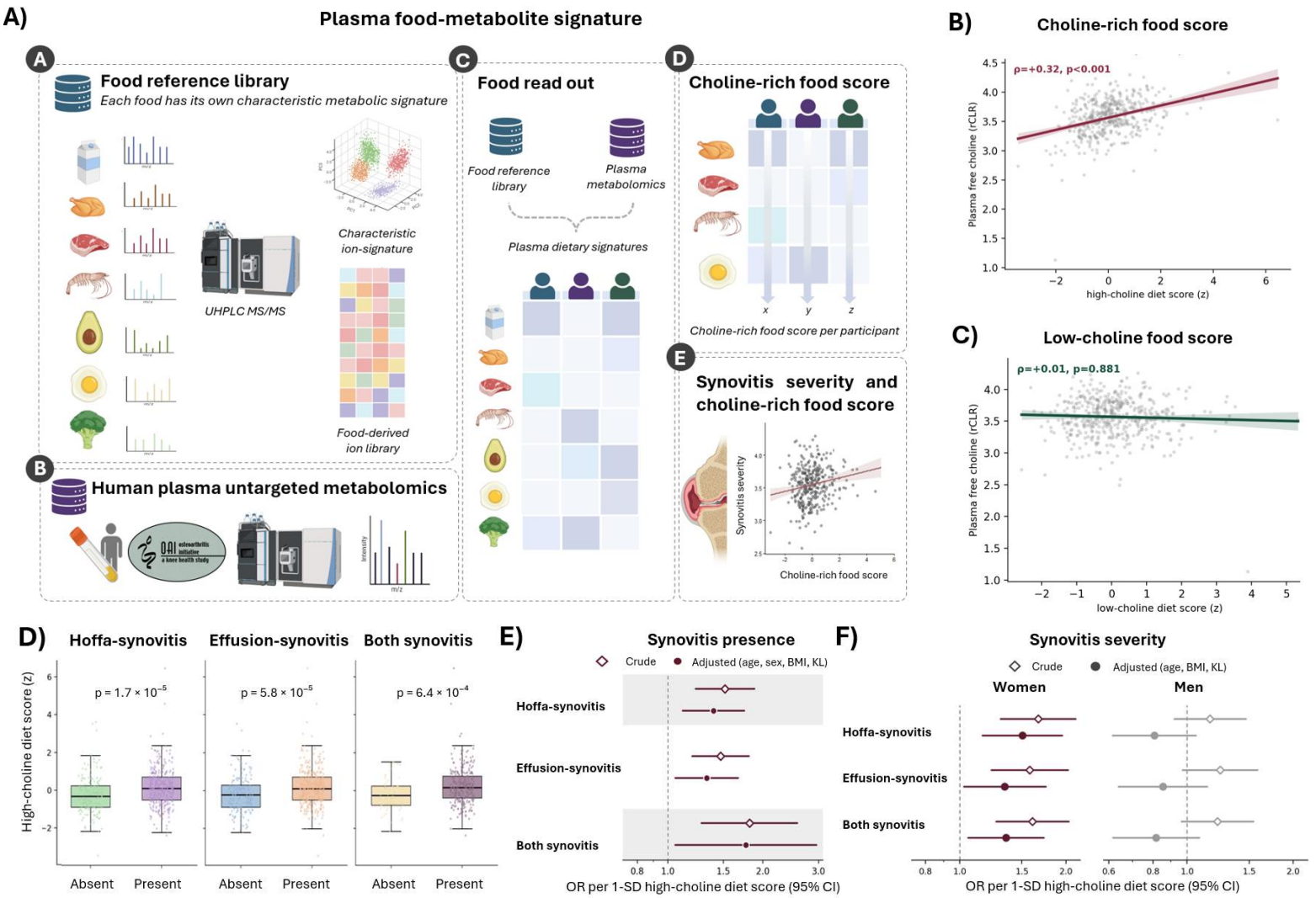


Figure 2 | A plasma food-metabolite signature links dietary choline exposure to circulating choline and synovitis. (A) Workflow for plasma-based dietary profiling: MS/MS signatures from individual foods in a reference library were matched against untargeted plasma metabolomics from OAI participants to generate participant-specific food-class readouts. A choline-rich food score was derived from egg, meat (beef, veal and pork), poultry and seafood (salmon, langostino and tilapia), whereas a low-choline food score was derived from fruit, grains, seeds, vegetables and fungi and associated with synovitis presence and severity. (B) Association between the choline-rich food score and circulating free choline. (C) Association between the low-choline food score and circulating free choline. Lines indicate linear fits, and shaded bands indicate 95% confidence intervals. Spearman correlation coefficients and two-sided *P* values are shown. (D) Distribution of the choline-rich food score according to the presence or absence of synovitis phenotypes. Two-sided Wilcoxon *P* values are shown. Boxes indicate the median and interquartile range, and whiskers extend to 1.5 × IQR. (E) OR for synovitis presence per 1-SD increment in the choline-rich food score. Open symbols indicate crude estimates and filled symbols indicate estimates adjusted for age, sex, BMI and summed baseline radiographic KL grade of both knees. (F) Sex-stratified associations between the choline-rich food score and synovitis severity in women (n= 207) and men (n= 138), estimated using ordinal logistic regression. Odds ratios are expressed per 1-SD increment in the score. Open symbols indicate crude estimates and filled symbols indicate estimates adjusted for age, BMI and summed baseline KL grade. Bars indicate 95% confidence intervals. BL, baseline; BMI, body mass index; CI, confidence interval; KL, Kellgren–Lawrence; OAI, Osteoarthritis Initiative; OR, odds ratio.

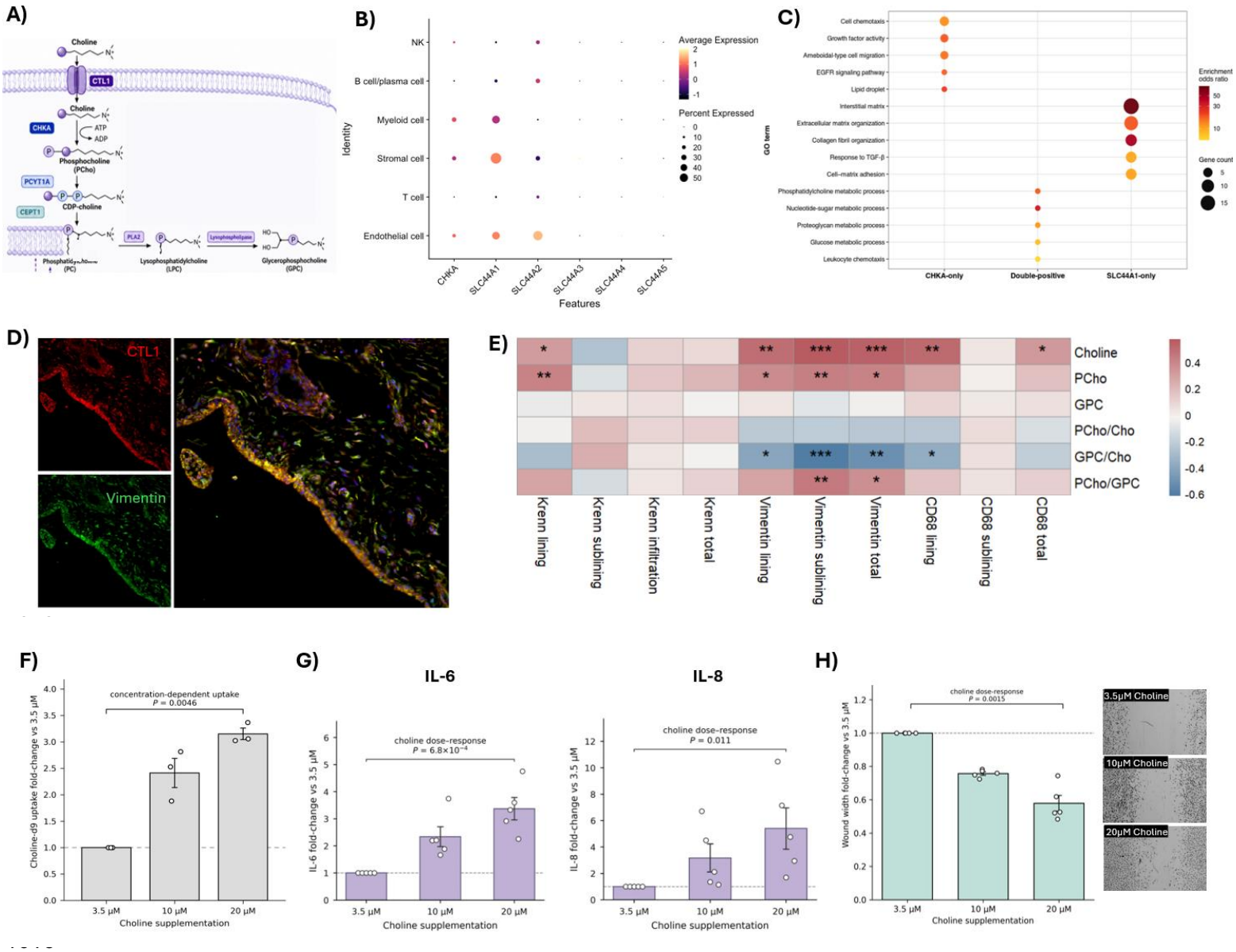


Figure 3 | The choline–phosphocholine axis promotes inflammatory and migratory responses in OA synovial fibroblasts. (A) Schematic of the choline pathway, including CTL1-mediated choline uptake, phosphorylation to phosphocholine (PCho) by ChoKα, and incorporation into phosphatidylcholine (PC) through the Kennedy pathway for membrane phospholipid synthesis. PC degradation generates glycerophosphocholine (GPC), representing the degradative arm of membrane phospholipid turnover. (B) Single-cell RNA-sequencing analysis of SLC44-family transporters and CHKA across human OA synovial cell populations (n = 9). (C) Gene ontology enrichment in SLC44A1- and CHKA-expressing OA synovial fibroblasts. (D) Representative dual immunofluorescence for CTL1 and vimentin (N=4). (E) Associations of synovial choline, phosphocholine (PCho), glycerophosphocholine (GPC), and their ratios with histological features in synovial biopsies analyzed by ^1H NMR metabolomics (n = 36). (F) Concentration-dependent uptake of isotopically labelled choline-d9 by FLS after 10 min. (G) IL-8 and IL-6 secretion following supplementation with 3.5–20 µM choline (n= 5). Responses are expressed relative to the 0 µM condition; dose–response effects were assessed using patient-specific log–log slopes. (H) FLS migration following choline supplementation (n= 5). FLS, fibroblast-like synoviocytes; PCho, phosphocholine; GPC, glycerophosphocholine.

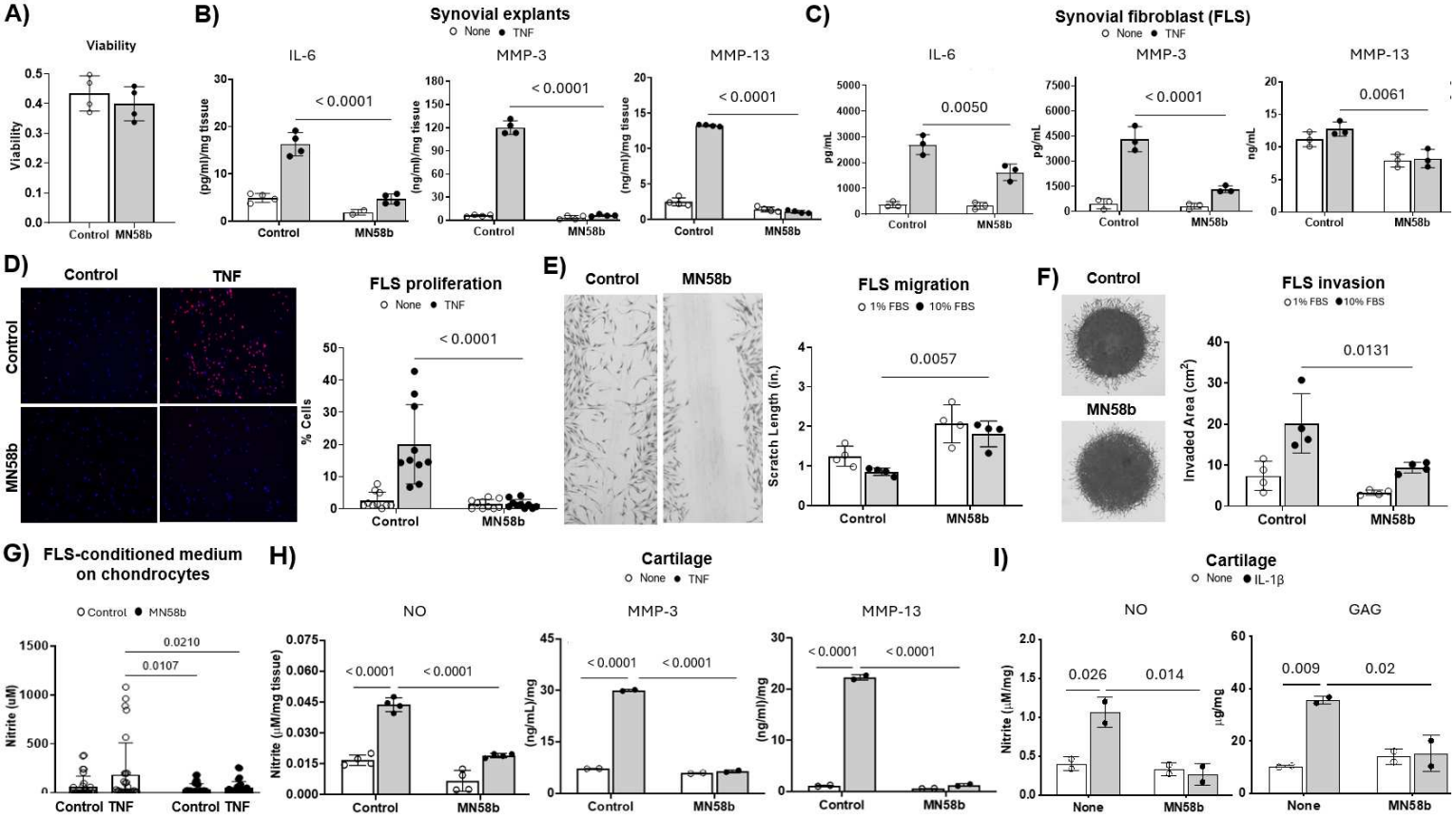


Figure 4. ChoKα inhibition attenuates pathogenic FLS behavior and protects cartilage from FLS-driven and direct catabolism in vitro. (A) Viability of human OA fibroblast-like synoviocytes (FLS) treated with vehicle (Control) or the ChoKα inhibitor MN58b (5 µM, 24 h) (n =4 donors). (B) IL-6, MMP-3 and MMP-13 secretion by human OA synovial explants (n = 4 donors) and (C) OA FLS, treated with vehicle or MN58b under basal (None, open symbols) or TNF–stimulated (filled symbols) conditions (n = 3 donors). (D) FLS proliferation assessed by EdU incorporation under basal and TNF-α–stimulated conditions; representative immunofluorescence images showing EdU^+ nuclei (red) and total nuclei (DAPI, blue), with quantification of the percentage of EdU^+ cells (n =10 donors). (E) FLS migration assessed by scratch/wound-healing assay in DMEN 1% vs 10% FBS; representative images and quantification (scratch length) (n =4 donors). (F) FLS invasion assessed by spheroid invasion assay in 1% vs 10% FBS; representative images and quantification (invaded area) (n =4 donors). (G) Nitrite release by primary OA chondrocytes after 24 h exposure to conditioned medium collected from donor-matched FLS treated for 24 h with vehicle (control) or MN58b under basal or TNF–stimulated conditions (n = 5 donors). (H) NO (nitrite), MMP-3 and MMP-13 release from human OA cartilage explants (n =4 donors) stimulated with TNF in the presence or absence of MN58b, and (I) NO and GAG release from OA cartilage explants (n =2 donors) stimulated with IL-1β in the presence or absence of MN58b. Data are presented as mean ± SD. Data in H and I were normalized with weight of cartilage explants. FLS, fibroblast-like synoviocytes; ChoKα, choline kinase α; NO, nitric oxide; GAG, glycosaminoglycan; MMP, matrix metalloproteinase; FBS, fetal bovine serum; EdU, 5-ethynyl-2′-deoxyuridine; OA, osteoarthritis.

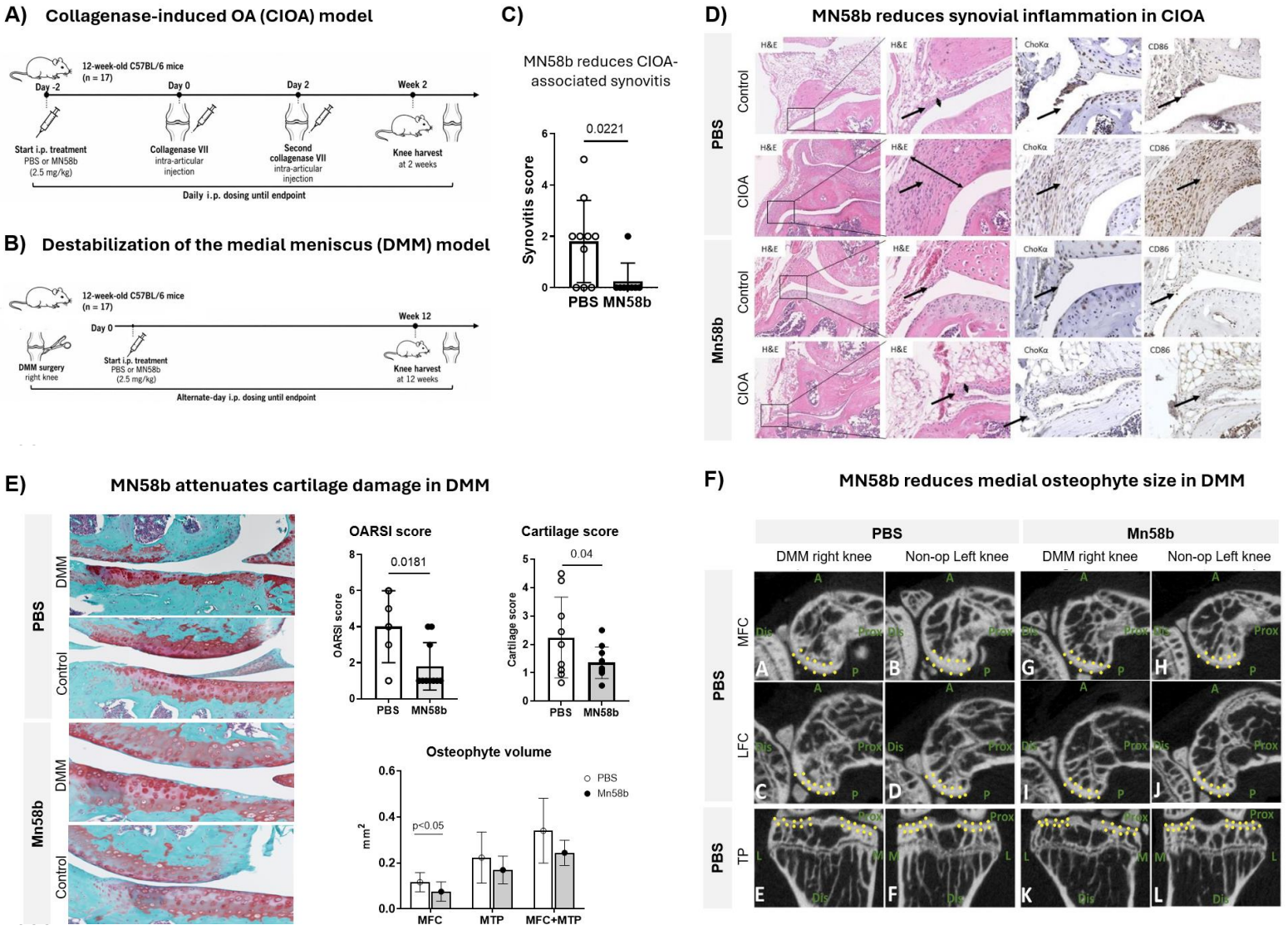


Figure 5 | Pharmacological ChoKα inhibition attenuates synovitis and structural joint damage in vivo. (A) Experimental design of the collagenase-induced osteoarthritis (CIOA) model. (B) Experimental design of the destabilization of the medial meniscus (DMM) model. (C) Histological synovitis scores in PBS- and MN58b-treated CIOA mice. (D) Representative H&E and immunohistochemical staining for ChoKα and CD68 in control and CIOA knees from PBS- and MN58b-treated mice. Arrows indicate synovial thickening and positive staining. (E) Representative Safranin O–Fast Green-staining and quantification of OARSI score, cartilage damage score and osteophyte volume in DMM mice. Each point represents one mouse; bars show mean ± SD. (F) Representative µCT images of DMM-operated right knees and contralateral non-operated left knees from PBS- and MN58b-treated mice. Yellow dashed lines delineate medial osteophytes. MFC, medial femoral condyle; LFC, lateral femoral condyle; MTP, medial tibial plateau; LTP, lateral tibial plateau; Non-Op, non-operated.

REFERENCES

1. Hunter, D.J. & Bierma-Zeinstra, S. Osteoarthritis. *Lancet* **393**, 1745-1759 (2019).
2. Long, H. *et al.* Prevalence Trends of Site-Specific Osteoarthritis From 1990 to 2019: Findings From the Global Burden of Disease Study 2019. *Arthritis Rheumatol* **74**, 1172-1183 (2022).
3. Loeser, R.F., Goldring, S.R., Scanzello, C.R. & Goldring, M.B. Osteoarthritis: a disease of the joint as an organ. *Arthritis Rheum* **64**, 1697-1707 (2012).
4. Berenbaum, F. Osteoarthritis as an inflammatory disease (osteoarthritis is not osteoarthrosis!). *Osteoarthritis Cartilage* **21**, 16-21 (2013).
5. Felson, D.T. *et al.* Synovitis and the risk of knee osteoarthritis: the MOST Study. *Osteoarthritis Cartilage* **24**, 458-464 (2016).
6. Sanchez-Lopez, E., Coras, R., Torres, A., Lane, N.E. & Guma, M. Synovial inflammation in osteoarthritis progression. *Nat Rev Rheumatol* **18**, 258-275 (2022).
7. Sellam, J. & Berenbaum, F. The role of synovitis in pathophysiology and clinical symptoms of osteoarthritis. *Nat Rev Rheumatol* **6**, 625-635 (2010).
8. Moulin, D., Sellam, J., Berenbaum, F., Guicheux, J. & Boutet, M.A. The role of the immune system in osteoarthritis: mechanisms, challenges and future directions. *Nat Rev Rheumatol* **21**, 221-236 (2025).
9. Hill, C.L. *et al.* Synovitis detected on magnetic resonance imaging and its relation to pain and cartilage loss in knee osteoarthritis. *Ann Rheum Dis* **66**, 1599-1603 (2007).
10. Roemer, F.W. *et al.* Presence of MRI-detected joint effusion and synovitis increases the risk of cartilage loss in knees without osteoarthritis at 30-month follow-up: the MOST study. *Ann Rheum Dis* **70**, 1804-1809 (2011).
11. Atukorala, I. *et al.* Synovitis in knee osteoarthritis: a precursor of disease? *Ann Rheum Dis* **75**, 390-395 (2016).
12. Murillo-Saich, J.D. *et al.* Synovial tissue metabolomic profiling reveal biomarkers of synovial inflammation in patients with osteoarthritis. *Osteoarthr Cartil Open* **4**, 100295 (2022).
13. Berenbaum, F., Wallace, I.J., Lieberman, D.E. & Felson, D.T. Modern-day environmental factors in the pathogenesis of osteoarthritis. *Nat Rev Rheumatol* **14**, 674-681 (2018).
14. Courties, A., Berenbaum, F. & Sellam, J. The Phenotypic Approach to Osteoarthritis: A Look at Metabolic Syndrome-Associated Osteoarthritis. *Joint Bone Spine* **86**, 725-730 (2019).
15. De Roover, A., Escribano-Nunez, A., Monteagudo, S. & Lories, R. Fundamentals of osteoarthritis: Inflammatory mediators in osteoarthritis. *Osteoarthritis Cartilage* **31**, 1303-1311 (2023).
16. Gauglitz, J.M. *et al.* Enhancing untargeted metabolomics using metadata-based source annotation. *Nat Biotechnol* **40**, 1774-1779 (2022).
17. Dorrestein, P. *et al.* Learning molecular fingerprints of foods to decode dietary intake. *Res Sq* (2025).
18. Guma, M. *et al.* Choline kinase inhibition in rheumatoid arthritis. *Ann Rheum Dis* **74**, 1399-1407 (2015).
19. Collaborators, G.B.D.O. Global, regional, and national burden of osteoarthritis, 1990-2020 and projections to 2050: a systematic analysis for the Global Burden of Disease Study 2021. *Lancet Rheumatol* **5**, e508-e522 (2023).
20. Tang, S. *et al.* Osteoarthritis. *Nat Rev Dis Primers* **11**, 10 (2025).
21. Snider, S.A. *et al.* Choline transport links macrophage phospholipid metabolism and inflammation. *J Biol Chem* **293**, 11600-11611 (2018).
22. Sanchez-Lopez, E. *et al.* Choline Uptake and Metabolism Modulate Macrophage IL-1beta and IL-18 Production. *Cell Metab* **29**, 1350-1362 e1357 (2019).
23. Xu, S. *et al.* Metabolomic Signatures of Dietary Patterns and Incident Radiographic Knee Osteoarthritis: A Case-Cohort Study From the Osteoarthritis Initiative. *J Rheumatol* **53**, 443-449 (2026).
24. Liu, T. *et al.* Whole grain consumption and risk of radiographic knee osteoarthritis: a prospective study from the Osteoarthritis Initiative. *Rheumatology (Oxford)* **62**, 1834-1840 (2023).
25. Xu, C. *et al.* Dietary patterns and risk of developing knee osteoarthritis: data from the osteoarthritis initiative. *Osteoarthritis Cartilage* **29**, 834-840 (2021).
26. Wu, L. *et al.* Association between Iron Intake and Progression of Knee Osteoarthritis. *Nutrients* **14** (2022).
27. Horace, R.W. *et al.* The association between vitamin K and medial tibial-femoral knee osteoarthritis progression: Data from the osteoarthritis initiative. *Osteoarthr Cartil Open* **3**, 100172 (2021).

28. Xu, C. *et al.* Dietary Patterns and Progression of Knee Osteoarthritis: Data from the Osteoarthritis Initiative. *Am J Clin Nutr* **111**, 667-676 (2020).
29. Joseph, G.B. *et al.* Associations Between Vitamins C and D Intake and Cartilage Composition and Knee Joint Morphology Over 4 Years: Data From the Osteoarthritis Initiative. *Arthritis Care Res (Hoboken)* **72**, 1239-1247 (2020).
30. Shmagel, A. *et al.* Low magnesium intake is associated with increased knee pain in subjects with radiographic knee osteoarthritis: data from the Osteoarthritis Initiative. *Osteoarthritis Cartilage* **26**, 651-658 (2018).
31. Veronese, N. *et al.* Mediterranean diet and knee osteoarthritis outcomes: A longitudinal cohort study. *Clin Nutr* **38**, 2735-2739 (2019).
32. Veronese, N. *et al.* The relationship between the dietary inflammatory index and prevalence of radiographic symptomatic osteoarthritis: data from the Osteoarthritis Initiative. *Eur J Nutr* **58**, 253-260 (2019).
33. Kenny, T.C., Scharenberg, S., Abu-Remaileh, M. & Birsoy, K. Cellular and organismal function of choline metabolism. *Nat Metab* **7**, 35-52 (2025).
34. Trujillo-Gonzalez, I. *et al.* Choline and betaine concentrations in plasma discriminate levels of dietary choline intake in healthy adults: analysis of a double-blind randomized crossover controlled feeding study. *Am J Clin Nutr* **123**, 101236 (2026).
35. Paz-Gonzalez, R. *et al.* An Atlas of the Knee Joint Proteins and Their Role in Osteoarthritis Defined by Literature Mining. *Mol Cell Proteomics* **22**, 100606 (2023).
36. Ishibashi, K. *et al.* Detection of synovitis in early knee osteoarthritis by MRI and serum biomarkers in Japanese general population. *Sci Rep* **10**, 12310 (2020).
37. Sasaki, E. *et al.* Metabolomics with severity of radiographic knee osteoarthritis and early phase synovitis in middle-aged women from the Iwaki Health Promotion Project: a cross-sectional study. *Arthritis Res Ther* **24**, 145 (2022).
38. Murillo-Saich, J.D. *et al.* Potential role of bile acids as a microbiome-derived mechanism in synovitis of knee osteoarthritis synovitis. *Osteoarthritis Cartilage* **34**, 794-805 (2026).
39. Fischer, L.M., da Costa, K.A., Kwock, L., Galanko, J. & Zeisel, S.H. Dietary choline requirements of women: effects of estrogen and genetic variation. *Am J Clin Nutr* **92**, 1113-1119 (2010).
40. Akkaya, Z. *et al.* Ultra-processed food consumption is associated with knee osteoarthritis: Data from the Osteoarthritis Initiative. *Osteoarthritis Cartilage* **33**, 1130-1140 (2025).
41. Guerra, G. *et al.* Circulating choline and phosphocholine measurement by a hydrophilic interaction liquid chromatography-tandem mass spectrometry. *Heliyon* **9**, e21921 (2023).
42. Lester, G. The Osteoarthritis Initiative: A NIH Public-Private Partnership. *HSS J* **8**, 62-63 (2012).
43. Hunter, D.J., Nevitt, M., Losina, E. & Kraus, V. Biomarkers for osteoarthritis: current position and steps towards further validation. *Best Pract Res Clin Rheumatol* **28**, 61-71 (2014).
44. Hunter, D. *et al.* Longitudinal validation of periarticular bone area and 3D shape as biomarkers for knee OA progression? Data from the FNIH OA Biomarkers Consortium. *Ann Rheum Dis* **75**, 1607-1614 (2016).
45. Roemer, F.W. *et al.* A perspective on the evolution of semi-quantitative MRI assessment of osteoarthritis: Past, present and future. *Osteoarthritis Cartilage* **32**, 460-472 (2024).
46. Hunter, D.J. *et al.* Evolution of semi-quantitative whole joint assessment of knee OA: MOAKS (MRI Osteoarthritis Knee Score). *Osteoarthritis Cartilage* **19**, 990-1002 (2011).
47. Rosset, A., Spadola, L. & Ratib, O. OsiriX: an open-source software for navigating in multidimensional DICOM images. *J Digit Imaging* **17**, 205-216 (2004).
48. van Helvoort, E.M. *et al.* Cohort profile: The Applied Public-Private Research enabling OsteoArthritis Clinical Headway (IMI-APPROACH) study: a 2-year, European, cohort study to describe, validate and predict phenotypes of osteoarthritis using clinical, imaging and biochemical markers. *BMJ Open* **10**, e035101 (2020).
49. Roemer, F.W. *et al.* Structural tissue damage and 24-month progression of semi-quantitative MRI biomarkers of knee osteoarthritis in the IMI-APPROACH cohort. *BMC Musculoskelet Disord* **23**, 988 (2022).
50. Kessner, D., Chambers, M., Burke, R., Agus, D. & Mallick, P. ProteoWizard: open source software for rapid proteomics tools development. *Bioinformatics* **24**, 2534-2536 (2008).
51. Schmid, R. *et al.* Integrative analysis of multimodal mass spectrometry data in MZmine 3. *Nat Biotechnol* **41**, 447-449 (2023).
52. Rohart, F., Gautier, B., Singh, A. & Le Cao, K.A. mixOmics: An R package for 'omics feature selection and multiple data integration. *PLoS Comput Biol* **13**, e1005752 (2017).

53. Lau, E.S. *et al.* Eicosanoid and eicosanoid-related inflammatory mediators and exercise intolerance in heart failure with preserved ejection fraction. *Nat Commun* **14**, 7557 (2023).
54. Agongo, J. *et al.* Quantitative Food Compounds Enable Dietary Ontology Referencing across 500 Foods and Human Plasma. *Anal Chem* **98**, 3160-3176 (2026).
55. Fukagawa, N.K. *et al.* USDA's FoodData Central: what is it and why is it needed today? *Am J Clin Nutr* **115**, 619-624 (2022).
56. Zhang, F. *et al.* Deconstruction of rheumatoid arthritis synovium defines inflammatory subtypes. *Nature* **623**, 616-624 (2023).
57. Krenn, V. *et al.* [Low-grade-/high-grade-synovitis: synovitis-score as a gold standard?]. *Orthopade* **35**, 853-859 (2006).
58. Mussawy, H. *et al.* The histopathological synovitis score is influenced by biopsy location in patients with knee osteoarthritis. *Arch Orthop Trauma Surg* **142**, 2991-2997 (2022).
59. Schindelin, J. *et al.* Fiji: an open-source platform for biological-image analysis. *Nat Methods* **9**, 676-682 (2012).

Supplementary Files

This is a list of supplementary files associated with this preprint. Click to download.

- NatCommunSupplementaryInformation.pdf